

Bulk-surface virtual element method for systems of coupled bulk-surface PDEs in two-space dimensions

Massimo Frittelli*, Anotida Madzvamuse†, Ivonne Sgura‡

Abstract

In this manuscript we present a novel bulk-surface virtual element method (BSVEM) for the numerical approximation of coupled systems of elliptic and parabolic bulk-surface partial differential equations (BSPDEs) in two dimensions. To the best of the authors' knowledge, the proposed method is the first application of the virtual element method [5] to BSPDEs. The BSVEM is based on the discretisation of the bulk domain into polygonal elements with arbitrarily many edges, rather than just triangles. The polygonal approximation of the bulk induces a piecewise linear approximation of the one-dimensional surface (a curve). The bulk-surface finite element method on triangular meshes [25] is a special case of the proposed method. The present work contains several contributions. First, we show that the proposed method has optimal second-order convergence in space, provided the exact solution is $H^{2+1/4}$ in the bulk and H^2 on the surface, where the additional $\frac{1}{4}$ is required by the combined effect of surface curvature and polygonal elements. Our analysis shows, as a by-product, that first-degree virtual elements for bulk-only PDEs retain optimal convergence in the presence of surface curvature. In carrying out the analysis we provide novel theoretical tools for the analysis of curved boundaries and non-constant boundary conditions, such as the Sobolev extension and a special inverse trace operator. We show that general polygons can be exploited to reduce the computational complexity of the matrix assembly. Moreover, we present an optimised matrix implementation that can also be exploited in the pre-existing special case of bulk-surface finite elements on triangular meshes [25]. Numerical examples illustrate our findings and experimentally show the optimal convergence rates in space and time.

1 Introduction

In this work, we present for the first time, the bulk-surface virtual element method (BSVEM) which is a substantial extension of the virtual element method (VEM). The VEM is a recent extension of the well-known finite element method (FEM) for the numerical approximation of several classes of partial differential equations on flat domains [5] or surfaces [29]. The key feature of VEM is that of being a *polygonal* method, i.e. it handles elements of a quite general polygonal shape, rather than just

*University of Salento, Department of Innovation Engineering, Via per Monteroni, 73100 Lecce (Italy). Email: massimo.frittelli@unisalento.it

†University of Sussex, School of Mathematical and Physical Sciences, Department of Mathematics, BN1 9QH, Brighton, UK and University of Johannesburg, Department of Mathematics, South Africa. Email: A.Madzvamuse@sussex.ac.uk

‡University of Salento, Department of Mathematics and Physics "E. De Giorgi", Via per Arnesano, 73100 Lecce (Italy). Email: ivonne.sgura@unisalento.it

of triangular shape [5]. The success of virtual elements is due to several advantages arising from non-polygonal mesh generality. A non-exhaustive list of such advantages includes: (i) computationally cheap mesh pasting [12, 18, 29], (ii) efficient adaptive algorithms [17], flexible approximation of the domain and in particular of its boundary [22], and the possibility of enforcing higher regularity to the numerical solution [4, 9, 15], just to mention a few. Thanks to these advantages, several extensions of the original VEM for the Poisson equation [5] were developed for numerous PDE problems, such as heat [44] and wave equations [43], reaction-diffusion systems [1], Cahn-Hilliard equation [4], Stokes equation [8], linear elasticity [6], plate bending [15], fracture problems [11], eigenvalue problems [37] and many more.

An interesting class of PDE problems that is recently drawing attention in the literature is that of *coupled bulk-surface partial differential equations* (BSPDEs). Given a number $d \in \mathbb{N}$ of space dimensions, a BSPDE is a system of $m \in \mathbb{N}$ PDEs posed in the *bulk* $\Omega \subset \mathbb{R}^d$ coupled with $n \in \mathbb{N}$ PDEs posed on the surface $\Gamma := \partial\Omega$ through either linear or non-linear coupling, see for instance [35]. The quickly growing interest toward BSPDEs arises from the numerous applications of such PDE problems in different areas, such as cellular biological systems [21, 27, 34, 38] or fluid dynamics [14, 16, 32], among many other applications.

Among the various state-of-the-art numerical methods for the spatial discretisation of BSPDEs existing in the literature we mention finite elements [25, 31, 35, 36], trace finite elements [30], cut finite elements [16] and discontinuous Galerkin methods [19]. The purpose of the present paper is to introduce a *bulk-surface virtual element method* (BSVEM) for the spatial discretisation of a coupled system of BSPDEs in two space dimensions. The proposed method combines the VEM for the bulk equation(s) with the surface finite element method (SFEM) for the surface equation(s). We apply the proposed method to (i) the linear elliptic bulk-surface Poisson problem considered in [25] and (ii) a class of bulk-surface reaction-diffusion systems (BSRDSs) with non-linear coupling that covers several models addressed in the literature, see for instance [21, 27, 35].

The main novelty in the present study is devoted to error analysis. In fact, the simultaneous presence of non-triangular elements and boundary approximation error (which cannot be neglected in the context of BSPDEs) provides new numerical analysis challenges. We prove that the proposed method possesses optimal second-order convergence in space, provided the exact solution is $H^{2+1/4}$ in the bulk and H^2 on the surface. This is slightly more than the usual requirement of H^2 both in the bulk and on the surface [31]. However, our analysis requires this slightly higher regularity assumption only *in the simultaneous presence of a curved boundary Γ and non-triangular elements close to the boundary*, which is a novel case. Otherwise, our results fall back to the known cases in the literature, see for instance [31] for the case of triangular BSFEM and [1] for the case of polygonal VEM in the absence of curvature in the boundary Γ .

As a by-product of the error analysis, we show that the bulk-VEM of lowest polynomial order $k = 1$ possesses optimal convergence also *in the presence of curved boundaries*. A first work in this direction is found in [10], in which the authors consider polygonal elements with a curved boundary that match the exact domain in order to take out the geometric error. Subsequently, in [13], the need of matching the exact domain was removed by introducing suitable corrections. In the present work, we obtain similar results in the low polynomial case $k = 1$ by using the geometric theory of BSPDEs.

A second by-product of the present study is a potential alternative approach to the *lifting operator* used in the analysis of SPDEs [24] and BSPDEs [25]: the Sobolev extension operator. In fact, we prove that, if a function is $H^{2+1/4}$ instead of H^2 in the two-dimensional bulk, the Sobolev extension retains the optimal approximation properties of lifting. Moreover, the Sobolev extension of a function has the property of preserving its $W^{m,p}$ class, while its lift does not. This property, which is crucial in our analysis, is potentially beneficial to the theory of numerical analysis of more general PDEs.

The third by-product of our error analysis is the existence of a special *inverse trace operator* that we use for accounting for general boundary conditions. Like the standard inverse trace operator, our inverse trace maps a function $v \in H^1(\Gamma)$ to a function $v_B \in H^1(\Omega)$ such that $\|v_B\|_{H^1(\Omega)} \leq C\|v\|_{H^1(\Gamma)}$, with C depending on the domain Ω . Our inverse trace has the stronger property that $\|v_B\|_{L^2(\Omega)} \leq C\|v\|_{L^2(\Gamma)}$ and $\|v_B\|_{H^1(\Omega)} \leq \|v\|_{H^1(\Gamma)}$. This means that the proposed operator preserves both L^2 and H^1 norms up to the same multiplicative constants, i.e. it is an L^2 -preserving inverse trace.

The proposed method has all the benefits of polygonal meshes, two of which will be illustrated in the present work. First, the usage of suitable polygons drastically reduces the computational complexity of matrix assembly on equal meshsize in comparison to the triangular BSFEM. Similar results are obtained in the literature through other methods, such as trace FEMs [30] or cut FEMs [16]. Second, a curved portion of the boundary can be approximated with a single element with many edges. The BSVEM lends itself to other advantages due to its polygonal nature, such as efficient algorithms for adaptivity or mesh pasting, see for instance [17]. These aspects will be addressed in future studies.

Hence, the structure of our paper is as follows. In Section 2, we introduce the model equations to be addressed in the present work, both in strong and weak formulations. In Section 3, we introduce polygonal bulk-surface meshes, analyse geometric error, define suitable function spaces, analyse their approximation properties and present the spatial discretisation of the considered BSPDE problems. In Section 4, we carry out the convergence error analysis for the parabolic case, the main result being optimal second-order spatial convergence in the L^2 norm, both in the bulk and on the surface. In Section 5 we present an IMEX-Euler time discretisation of the parabolic problem. In Section 6 we show that polygonal meshes can be exploited to significantly reduce the computational time of the matrix assembly. In Section 7 we illustrate our findings through two numerical examples. The first experiment is on the elliptic problem and shows (i) the computational advantage in matrix assembly and (ii) optimal convergence in space. The second experiment shows the application of BSVEM-IMEX Euler scheme to the wave pinning reaction-diffusion model considered in [21]. In Appendix A we provide some basic definitions and results required in our analysis. In Appendix B we report some lengthy proofs involved in Section 4.

2 Coupled bulk-surface partial differential equations

2.1 Systems of coupled bulk-surface PDEs

Let $u(\mathbf{x})$ and $v(\mathbf{x})$ be the bulk and surface variables obeying the following elliptic *coupled bulk-surface problem*:

$$\begin{cases} -\Delta u(\mathbf{x}) + u(\mathbf{x}) = f(\mathbf{x}), & \mathbf{x} \in \Omega; \\ -\Delta_\Gamma v(\mathbf{x}) + v(\mathbf{x}) + \frac{\partial u}{\partial \boldsymbol{\nu}}(\mathbf{x}) = g(\mathbf{x}), & \mathbf{x} \in \Gamma; \\ \frac{\partial}{\partial \boldsymbol{\nu}} u(\mathbf{x}) = -\alpha u(\mathbf{x}) + \beta v(\mathbf{x}), & \mathbf{x} \in \Gamma, \end{cases} \quad (1)$$

where $\alpha, \beta > 0$. In the above, Δ and Δ_Γ denote the Laplace and Laplace-Beltrami operators respectively, while $\boldsymbol{\nu}$ denotes the outward unit normal vector field on Γ (see Appendix A for notations and definitions). The above model (1) was considered in [25] and can be seen as the simplest case of a bulk-surface PDE model. It is a linear elliptic bulk PDE coupled with a linear elliptic surface PDE through linear boundary conditions.

As a nonlinear time-dependent generalisation, let $u(\mathbf{x}, t)$ and $v(\mathbf{x}, t)$ be the bulk and surface

variables obeying the following *bulk-surface reaction-diffusion system*:

$$\begin{cases} \frac{\partial u}{\partial t}(\mathbf{x}, t) - d_u \Delta u(\mathbf{x}, t) = q(u(\mathbf{x}, t)), & \mathbf{x} \in \Omega, t \in [0, T]; \\ \frac{\partial v}{\partial t}(\mathbf{x}, t) - d_v \Delta_\Gamma v(\mathbf{x}, t) + \frac{\partial u}{\partial \boldsymbol{\nu}}(\mathbf{x}, t) = r(u(\mathbf{x}, t), v(\mathbf{x}, t)), & \mathbf{x} \in \Gamma, t \in [0, T]; \\ \frac{\partial u}{\partial \boldsymbol{\nu}}(\mathbf{x}, t) = s(u(\mathbf{x}, t), v(\mathbf{x}, t)), & \mathbf{x} \in \Gamma, t \in [0, T], \end{cases} \quad (2)$$

where T is the final time and $q(u), r(u, v), s(u, v)$ are possibly nonlinear functions. The above problem (2) can be seen as a semilinear reaction-diffusion equation for the bulk Ω coupled with a semilinear reaction-diffusion equation on the curve Γ through nonlinear boundary conditions given by $s(u, v)$. The model comprises several time-dependent bulk-surface PDE models existing in the literature, see for example [27, 35, 39]. We observe that problem (2) can be generalized by considering *evolving* bulk-surface domains. Such a generalized reaction-diffusion bulk-surface model would comprise additional models addressed in the literature, such as [33]. In this work, we focus only on models posed on stationary domains and leave the case of evolving domains for future work.

2.2 Weak formulations

In this section we state the weak formulations of the elliptic (1) and parabolic problems (2), respectively. For problem (1), we multiply the first two equations of (1) by two test functions $\varphi \in H^1(\Omega)$ and $\psi \in H^1(\Gamma)$, respectively, then we apply Green's formula in the bulk Ω and Green's formula on the one-dimensional manifold Γ [24]. We obtain the following formulation: find $u \in H^1(\Omega)$ and $v \in H^1(\Gamma)$ such that

$$\begin{cases} \int_{\Omega} \nabla u \cdot \nabla \varphi + \int_{\Omega} u \varphi = \int_{\Omega} f \varphi + \int_{\Gamma} \frac{\partial u}{\partial \boldsymbol{\nu}} \varphi; \\ \int_{\Gamma} \nabla_\Gamma v \cdot \nabla_\Gamma \psi + \int_{\Gamma} v \psi + \int_{\Gamma} \frac{\partial u}{\partial \boldsymbol{\nu}} \psi = \int_{\Gamma} g \psi, \end{cases} \quad (3)$$

for all $\varphi \in H^1(\Omega)$ and $\psi \in H^1(\Gamma)$. By using the third equation of (1) in (3), we obtain the following weak formulation: find $u \in H^1(\Omega)$ and $v \in H^1(\Gamma)$ such that

$$\begin{cases} \int_{\Omega} \nabla u \cdot \nabla \varphi + \int_{\Omega} u \varphi + \int_{\Gamma} (\alpha u - \beta v) \varphi = \int_{\Omega} f \varphi; \\ \int_{\Gamma} \nabla_\Gamma v \cdot \nabla_\Gamma \psi + \int_{\Gamma} (-\alpha u + (\beta + 1)v) \psi = \int_{\Gamma} g \psi, \end{cases} \quad (4)$$

for all $\varphi \in H^1(\Omega)$ and $\psi \in H^1(\Gamma)$. By reasoning similarly to the elliptic problem (1), we obtain the following weak formulation of the parabolic problem (2): find $u \in L^\infty([0, T]; H^1(\Omega))$ and $v \in L^\infty([0, T]; H^1(\Gamma))$ such that

$$\begin{cases} \int_{\Omega} \frac{\partial u}{\partial t} \varphi + d_u \int_{\Omega} \nabla u \cdot \nabla \varphi = \int_{\Omega} q(u) \varphi + \int_{\Gamma} s(u, v) \varphi; \\ \int_{\Gamma} \frac{\partial v}{\partial t} \psi + d_v \int_{\Gamma} \nabla_\Gamma v \cdot \nabla_\Gamma \psi + \int_{\Gamma} s(u, v) \psi = \int_{\Gamma} r(u, v) \psi, \end{cases} \quad (5)$$

for all $\varphi \in L^\infty([0, T]; H^1(\Omega))$ and $\psi \in L^\infty([0, T]; H^1(\Gamma))$. The following theorem contains existence, uniqueness and regularity results for the weak problem (4).

Theorem 1 (Existence, uniqueness and regularity for problem (4)). *If Γ is a \mathcal{C}^3 surface, $f \in L^2(\Omega)$ and $g \in L^2(\Gamma)$, then the weak elliptic problem (4) has a unique solution $(u, v) \in H^2(\Omega) \times H^2(\Gamma)$ that fulfils*

$$\|(u, v)\|_{H^2(\Omega) \times H^2(\Gamma)} \leq C \|(f, g)\|_{L^2(\Omega) \times L^2(\Gamma)}; \quad (6)$$

$$\|\text{Tr}(u)\|_{H^{3/2}(\Omega)} \leq C \|(f, g)\|_{L^2(\Omega) \times L^2(\Gamma)}, \quad (7)$$

where $C > 0$ is a constant that depends on α, β and Ω .

Proof. See [25] for estimate (6). Estimate (7) follows from (6) by using the trace inequality (A.11). \square

The problem of existence, uniqueness and regularity for the parabolic problem (5) is much more complicated and strictly depends on the nature of the kinetics $q(\cdot), r(\cdot)$ and of the coupling kinetics $s(\cdot)$. For the remainder of this work we will adopt the following set of assumptions.

Assumption 1 (Existence, uniqueness and regularity for problem (5)). *We assume that:*

- Γ is a \mathcal{C}^3 surface, q, r, s are \mathcal{C}^2 and globally Lipschitz functions.
- The initial datum (u_0, v_0) fulfils $u_0 \in H^2(\Omega)$, $\text{Tr}(u_0) \in H^2(\Gamma)$ and $v_0 \in H^2(\Gamma)$.
- There exists a unique solution (u, v) that fulfils

$$\begin{aligned} \|(u, \dot{u})\|_{L^\infty([0, T]; H^{2+1/4}(\Omega))} + \|(\text{Tr}(u), \text{Tr}(\dot{u}), v, \dot{v})\|_{L^\infty([0, T]; H^2(\Gamma))} \\ \leq C \exp(T) \left(\|u_0\|_{H^{2+1/4}(\Omega)} + \|(\text{Tr}(u_0), v_0)\|_{H^2(\Gamma)} \right), \end{aligned} \quad (8)$$

where $T > 0$ is the final time and $C > 0$ depends on Ω , $\|q\|_{\mathcal{C}^2(\mathbb{R})}$, $\|r\|_{\mathcal{C}^2(\mathbb{R}^2)}$ and $\|s\|_{\mathcal{C}^2(\mathbb{R}^2)}$.

In many applications, assuming globally Lipschitz kinetics is too restrictive and an ad-hoc analysis is required, see for instance [27]. However, there are notable examples of BSRDS models with globally Lipschitz kinetics, such as the wave pinning model studied in [21] and considered in the numerical example in Section 7.2. From here onwards, we shall assume that the weak parabolic problem (5) has a unique and sufficiently regular solution.

3 The Bulk-Surface Virtual Element Method

The purpose of this work is to introduce the bulk-surface virtual element method (BSVEM) for elliptic and parabolic bulk-surface PDEs in two space dimensions. The proposed method combines the Virtual Element Method (VEM) for elliptic [5] and parabolic [1, 44] PDEs on flat stationary domains with the bulk-surface finite element method (BSFEM) for elliptic [25] and parabolic [27] bulk-surface PDEs. This means that:

- In the absence of the surface equation, the method reduces -up to a different treatment of the nonlinear terms- to the VEM for elliptic [5] and parabolic [1, 44] PDEs on flat stationary domains.
- In the absence of non-triangular elements, the method reduces to the BSFEM for elliptic [25] and parabolic [31] problems.
- The numerical analysis of the proposed method faces new challenges arising from the combined effect of boundary approximation and non-triangular elements.

We will show that the proposed method possesses the following advantages:

- The usage of arbitrary polygons can be exploited to reduce the computational load of matrix assembly in the construction of the discrete (or semi-discrete) problem.
- The usage of arbitrary polygons can be exploited to accurately approximate curved boundaries with fewer elements.
- We present a simple matrix formulation of the discrete or semi-discrete problem that requires the assembly of two kinds of stiffness matrices and two kinds of mass matrices, only. Such a formulation simplifies the approach utilised in [35], in which more matrices are used. Since the BSFEM is a special case of the proposed BSVEM, this study provides, as a by-product, an optimised implementation of the BSFEM.

In this section we will

- describe the polygonal bulk-surface meshes that will be used in the method;
- quantify the geometric error arising from polygonal approximation of bulk-surface domains;
- introduce the discrete function spaces used in the method and their approximation properties;
- introduce the discrete bulk- and surface bilinear forms used in the method;
- present the spatially discrete formulations of the elliptic- and parabolic problems (1) and (2), respectively.

3.1 Polygonal bulk-surface meshes

Let $h > 0$ be a positive number called *meshsize* and let $\Omega_h = \cup_{E \in \mathcal{E}_h} E$ be a polygonal approximation of the bulk Ω , where \mathcal{E}_h is a set of non-degenerate polygons. The polygonal bulk Ω_h automatically induces a piecewise linear approximation Γ_h of Γ , defined by $\Gamma_h = \partial\Omega_h$, exactly as in the case of triangular meshes, see for example [25]. Notice that we can write $\Gamma_h = \cup_{F \in \mathcal{F}_h} F$, where \mathcal{F}_h is the set of the edges of Ω_h that lie on Γ_h . We assume that:

- (F1) the diameter of each element $E \in \mathcal{E}_h$ does not exceed h ;
- (F2) for any two distinct elements $E_1, E_2 \in \mathcal{E}_h$, their intersection $E_1 \cap E_2$ is either empty, or a common vertex, or a common edge.
- (F3) all nodes of Γ_h lie on Γ ;
- (F4) every face $F \in \mathcal{F}_h$ is contained in the Fermi stripe U of Γ (see Fig. 1 for an illustration).
- (V1) there exists $\gamma_1 > 0$ such that every $E \in \mathcal{E}_h$ is star-shaped with respect to a ball of radius $\gamma_1 h_E$, where h_E is the diameter of E ;
- (V2) there exists $\gamma_2 > 0$ such that for all $E \in \mathcal{E}_h$, the distance between any two nodes of E is at least $\gamma_2 h_E$.

Assumptions (F1)-(F4) are standard in the SFEM literature, see for instance [24], while assumptions (V1)-(V2) are standard in the VEM literature, see for instance [5]. The combined assumptions (V1)-(F4) will prove sufficient in our bulk-surface setting. In the following definitions and results we provide the necessary theory for estimating the geometric error arising from the boundary approximation.

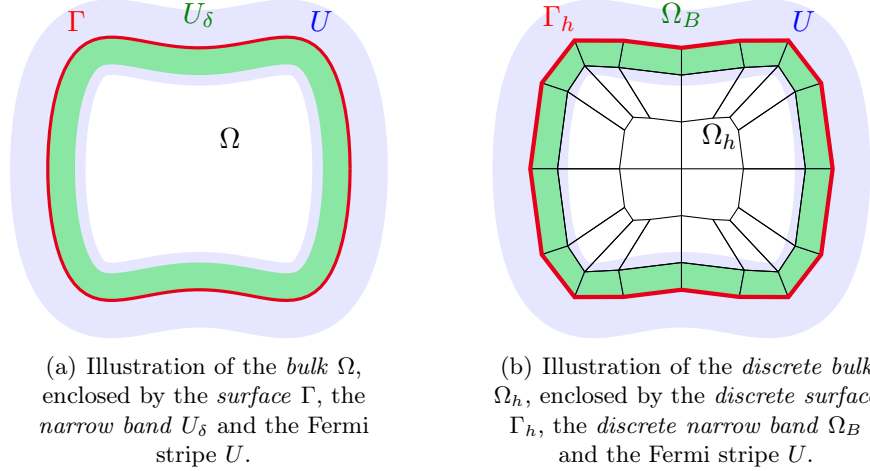


Figure 1: Illustration of continuous domain, discrete domain and related notations.

Definition 1 (Essentials of polygonal bulk-surface meshes). *An edge \bar{e} of any element $E \in \mathcal{E}_h$ is called a boundary edge if $\bar{e} \subset \Gamma_h$, otherwise \bar{e} is called an inner edge. Let $\mathcal{BE}(E)$ and $\mathcal{IE}(E)$ be the sets of boundary and inner edges of E , respectively. An element $E \in \mathcal{E}_h$ is called an exterior element if it has at least a boundary edge, otherwise E is called an interior element. Let Ω_B be the discrete narrow band defined as the union of the exterior elements of Ω_h as illustrated in Fig. 1(b). From Assumption (F4), for any boundary edge \bar{e} , we have that $\mathbf{a}(\bar{e}) \subset \Gamma$, where \mathbf{a} is the normal projection defined in Lemma (A1). Hence, for all $E \in \mathcal{E}_h$, we define the exact element \check{E} as the compact set enclosed by the edges $\mathcal{IE}(E) \cup \{\mathbf{a}(\bar{e}) | \bar{e} \in \mathcal{BE}(E)\}$, see Fig. 2 for an illustration.*

Remark 1 (Properties of polygonal bulk-surface meshes). *For any bulk-surface mesh (Ω_h, Γ_h) of meshsize $h > 0$ it holds that:*

- for sufficiently small $h > 0$, the discrete narrow band Ω_B is contained in the Fermi stripe U as shown in Fig. 1(b);
- the collection of all exact elements is a coverage of the exact bulk Ω , that is $\cup_{E \in \mathcal{E}_h} \check{E} = \Omega$.

Let $N \in \mathbb{N}$ and let \mathbf{x}_i , $i = 1, \dots, N$, be the nodes of Ω_h , which can be ordered in an arbitrary way. However, if Ω has a rectangular shape and the nodes are ordered along a Cartesian grid, the matrices associated with the method will have a block-tridiagonal structure. Let $M \in \mathbb{N}$, $M < N$ and assume that the nodes of Γ_h are \mathbf{x}_k , $k = 1, \dots, M$, i.e. the first M nodes of Ω_h . Throughout the paper we need the following *reduction matrix* $R \in \mathbb{R}^{N \times M}$ defined as $R := [I_M; 0]$, where I_M is the $M \times M$ identity matrix. Equivalently, $R = (r_{ik})$ is defined as

$$r_{ik} = \begin{cases} \delta_{ik} & \text{if } i = 1, \dots, M; \\ 0 & \text{if } i = M + 1, \dots, N, \end{cases} \quad (9)$$

for all $k = 1, \dots, M$, where δ_{ik} is the Kronecker symbol. The reduction matrix R fulfils the following two properties:

- For $\mathbf{v} \in \mathbb{R}^N$, $R^T \mathbf{v} \in \mathbb{R}^M$ is the vector with the first M entries of \mathbf{v} ;
- For $\mathbf{w} \in \mathbb{R}^M$, $R\mathbf{w} \in \mathbb{R}^N$ is the vector whose first M entries are those of \mathbf{w} and the other $N - M$ entries are 0.

In what follows, we will use the matrix R for an optimised implementation of the BSVEM.

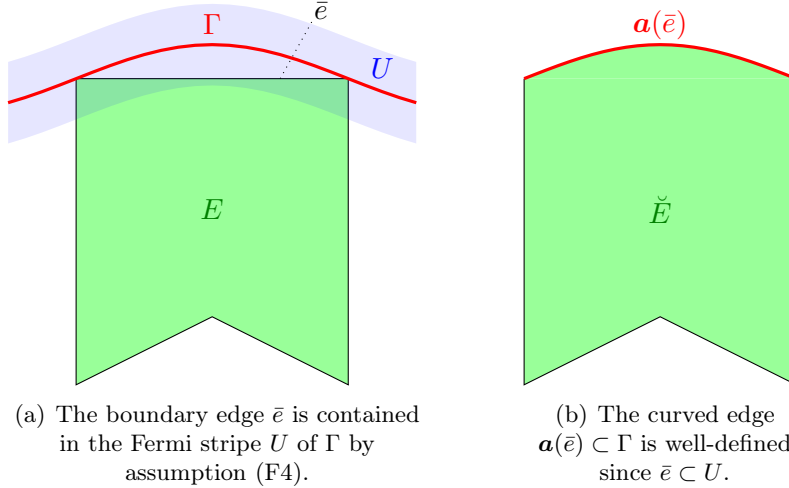


Figure 2: Construction of the exact element \check{E} corresponding to the polygonal element E according to Definition 1.

3.2 Variational crime

We now consider the geometric error due to the boundary approximation. Since the surface variational crime in surface finite elements is well-understood [24], we will mainly focus on the variational crime in the bulk. To this end, it is useful to analyse the relation between any element $E \in \mathcal{E}_h$ and its exact counterpart \check{E} , see Definition 1. For the special case of triangular meshes with at most one boundary edge per element, there exists a diffeomorphism between E and \check{E} and this diffeomorphism is linearly close to the identity with respect to the meshsize, see [25]. It is possible to show that, when E has more than three edges and/or multiple boundary edges, such a diffeomorphism might not exist, although a rigorous proof is beyond the scope of this paper. However, in the following result we show the existence of a mapping between E and \check{E} with slightly weaker regularity, which is sufficient for our purposes.

Lemma 1 (Parametrisation of the exact geometry). *Let \mathcal{E}_h fulfil assumptions (F1)-(V2). There exists a homeomorphism $G : \Omega_h \rightarrow \Omega$ such that $G \in W^{1,\infty}(\Omega_h)$ and*

$$G|_{\Gamma_h} = \mathbf{a}|_{\Gamma_h}; \quad (10)$$

$$G|_{\Omega_h \setminus \Omega_B} = Id; \quad (11)$$

$$\|JG - Id\|_{L^\infty(\Omega_B)} \leq Ch; \quad (12)$$

$$\|\det(JG) - 1\|_{L^\infty(\Omega_B)} \leq Ch; \quad (13)$$

$$\|G - Id\|_{L^\infty(\Omega_B)} \leq Ch^2, \quad (14)$$

where \mathbf{a} is the normal projection defined in Lemma A1, JG is the Jacobian of G and C is a constant that depends on Γ and the constants γ_1, γ_2 are those considered in Assumptions (V1)-(V2).

Proof. Let $E \in \mathcal{E}_h$. By Assumption (V2), E is star-shaped with respect to a ball \mathcal{B}_E of diameter $R_E \geq \gamma_2 h_E$, let \mathbf{x}_E be the center of such ball, see Fig. 3(a). For $\bar{e} \in \mathcal{BE}(E)$ let $T_{\bar{e}}$ be the triangle spanned by \bar{e} and \mathbf{x}_E , see Fig. 3(b). Let us now consider the collection of all the $T_{\bar{e}}$'s defined as follows: $\mathcal{BT}_h := \{T_{\bar{e}} | \bar{e} \in E, E \in \mathcal{E}_h\}$. We need to prove that \mathcal{BT}_h is quasi-uniform, i.e we need to

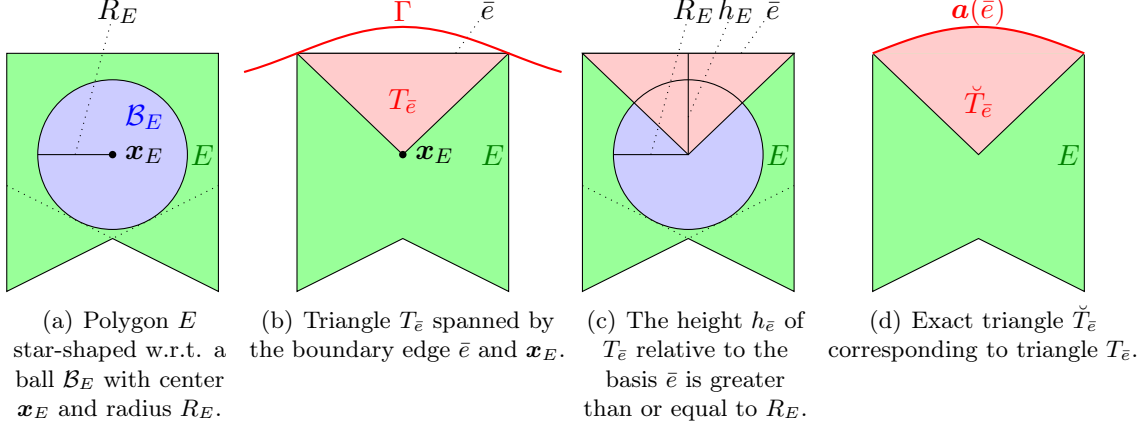


Figure 3: Some steps of the proof of Lemma 1.

prove that for all $E \in \mathcal{E}_h$ and $\bar{e} \in \mathcal{BE}(E)$, the triangle $T_{\bar{e}}$ has an inscribed ball of diameter greater or equal to $\bar{\gamma}h_E$, where the constant $\bar{\gamma} > 0$ depends on γ_1 and γ_2 , only. To this end, if $h_{\bar{e}}$ is the height of $T_{\bar{e}}$ relative to the basis \bar{e} as in Fig. 3(c), then we have

$$|h_{\bar{e}}| \geq R_E \geq \gamma_1 h_E, \quad \text{from Assumption (V1);} \quad (15)$$

$$|\bar{e}| \geq \gamma_2 h_E, \quad \text{from Assumption (V2).} \quad (16)$$

In addition, since no edge of $T_{\bar{e}}$ is longer than h_E , our claim follows.

Let now $\check{T}_{\bar{e}}$ be the curved triangle corresponding to $T_{\bar{e}}$, see Fig. 3(d). Since the triangulation \mathcal{BT}_h is quasi-uniform, then, from [25, Proposition 4.7 and its proof] there exists a diffeomorphism $G_{\bar{e}} : T_{\bar{e}} \rightarrow \check{T}_{\bar{e}}$ such that

$$G_{\bar{e}}(\mathbf{x}) = \mathbf{a}(\mathbf{x}), \quad \forall \mathbf{x} \in \bar{e}; \quad (17)$$

$$G_{\bar{e}}(\mathbf{x}) = \mathbf{x}, \quad \forall \mathbf{x} \in \partial T_{\bar{e}} \setminus \bar{e}; \quad (18)$$

$$\|JG_{\bar{e}} - Id\|_{L^\infty(T_{\bar{e}})} \leq Ch; \quad (19)$$

$$\|\det(JG_{\bar{e}}) - 1\|_{L^\infty(T_{\bar{e}})} \leq Ch; \quad (20)$$

$$\|G_{\bar{e}} - Id\|_{L^\infty(T_{\bar{e}})} \leq Ch^2, \quad (21)$$

where C depends only on $\bar{\gamma}$, which in turn depends only on γ_1 and γ_2 . We are ready to construct the mapping $G : \Omega_h \rightarrow \Omega$ as follows:

$$G(\mathbf{x}) = \begin{cases} G_{\bar{e}}(\mathbf{x}), & \text{if } \mathbf{x} \in T_{\bar{e}} \text{ for some } \bar{e} \in \mathcal{BE}(E), E \in \mathcal{E}_h; \\ \mathbf{x}, & \text{otherwise.} \end{cases} \quad (22)$$

Property (18) can now be rephrased by saying that G , restricted to any inner edge of Ω_h , is the identity. In addition, since all the $G_{\bar{e}}$'s are homeomorphisms, we obtain that G is a homeomorphism between Ω_h and Ω . Finally, from (17), (19), (20) and (22) we obtain the desired estimates (10)-(13). \square

Remark 2 (Virtual elements for bulk-only PDEs). *Lemma 1 has an important consequence in the analysis of boundary approximation for VEMs for the case of bulk PDEs. For triangular finite*

elements, boundary approximation is a well-understood topic, see for instance [20]. For VEMs, the first work in this direction is [10], in which a VEM on exact curved polygons is considered, in order to take out the geometric error. However, for low order VEMs on non-curved polygons, it is intuitively known that the geometric error does not prevent optimality. To the best of the authors' knowledge, the present study provides, as a by-product, the first rigorous proof of this fact.

Thanks to Lemma 1 it is possible to define bulk- and surface-lifting operators.

Definition 2 (Bulk- and surface-lifting operators). *Given $V : \Omega_h \rightarrow \mathbb{R}$ and $W : \Gamma_h \rightarrow \mathbb{R}$, their lifts are defined by*

$$V^\ell := V \circ G^{-1}; \quad \text{and} \quad W^\ell := W \circ G^{-1}, \quad (23)$$

respectively. Conversely, given $v : \Omega \rightarrow \mathbb{R}$ and $w : \Gamma \rightarrow \mathbb{R}$, their inverse lifts are defined by

$$v^{-\ell} := v \circ G; \quad \text{and} \quad w^{-\ell} := w \circ G, \quad (24)$$

respectively, with $G : \Omega_h \rightarrow \Omega$ being the mapping defined in Lemma 1.

Lemma 1 also enables us to show the equivalence of Sobolev norms under lifting as illustrated next.

Lemma 2 (Equivalence of norms under lifting). *There exists two constants $c_2 > c_1 > 0$ depending on Γ and γ_2 such that, for all $V : \Omega_h \rightarrow \mathbb{R}$ and for all $W : \Gamma_h \rightarrow \mathbb{R}$,*

$$c_1 \|V^\ell\|_{L^2(\Omega_h^\ell)} \leq \|V\|_{L^2(\Omega_h)} \leq c_2 \|V^\ell\|_{L^2(\Omega_h^\ell)}; \quad (25)$$

$$c_1 |V^\ell|_{H^1(\Omega_h^\ell)} \leq |V|_{H^1(\Omega_h)} \leq c_2 |V^\ell|_{H^1(\Omega_h^\ell)}; \quad (26)$$

$$c_1 \|W^\ell\|_{L^2(\Gamma)} \leq \|W\|_{L^2(\Gamma_h)} \leq c_2 \|W^\ell\|_{L^2(\Gamma)}; \quad (27)$$

$$c_1 |W^\ell|_{H^1(\Gamma)} \leq |W|_{H^1(\Gamma_h)} \leq c_2 |W^\ell|_{H^1(\Gamma)}. \quad (28)$$

Proof. Estimates (25)-(26) are found by using the map G introduced in Lemma 1 in the proof of [25, Proposition 4.9]. A proof of (27)-(28) can be found in [24, Lemma 4.2]. \square

We are ready to estimate the effect of lifting on bulk- and surface integrals.

Lemma 3 (Geometric error of lifting). *If $u, \varphi \in H^1(\Omega)$, then*

$$\left| \int_{\Omega} \nabla u \cdot \nabla \varphi - \int_{\Omega_h} \nabla u^{-\ell} \cdot \nabla \varphi^{-\ell} \right| \leq Ch |u|_{H^1(\Omega_B^\ell)} |\varphi|_{H^1(\Omega_B^\ell)}, \quad (29)$$

$$\left| \int_{\Omega} u \varphi - \int_{\Omega_h} u^{-\ell} \varphi^{-\ell} \right| \leq Ch \|u\|_{L^2(\Omega_B^\ell)} \|\varphi\|_{L^2(\Omega_B^\ell)}, \quad (30)$$

where C depends on Γ , γ_1 and γ_2 . If $v, \psi \in H^1(\Gamma)$, then

$$\left| \int_{\Gamma} \nabla_{\Gamma} v \cdot \nabla_{\Gamma} \psi - \int_{\Gamma_h} \nabla_{\Gamma_h} v^{-\ell} \cdot \nabla_{\Gamma_h} \psi^{-\ell} \right| \leq Ch^2 |v|_{H^1(\Gamma)} |\psi|_{H^1(\Gamma)}; \quad (31)$$

$$\left| \int_{\Gamma} v \psi - \int_{\Gamma_h} v^{-\ell} \psi^{-\ell} \right| \leq Ch^2 \|v\|_{L^2(\Gamma)} \|\psi\|_{L^2(\Gamma)}, \quad (32)$$

where C depends on Γ , γ_1 and γ_2 .

Proof. To prove (29)-(30) it is sufficient to use the bulk geometric estimates (11)-(13) in the proof of [25, Lemma 6.2]. A proof of (31)-(32) can be found in [24]. \square

Lemma 3 allows to rephrase integrals on the exact domain as integrals on the discrete domain, and vice-versa, up to a small error that is $O(h)$ in the bulk and $O(h^2)$ on the surface.

Remark 3 (Preservation of regularity under lifting). *For $E \in \mathcal{E}_h$ the inverse lift of an $H^2(\check{E})$ function is not, in general, $H^2(E)$, cf. Remark A1 and Lemma 1. This problem does not arise in the context of triangular bulk-surface finite elements in the presence of curved boundaries, see for instance [31], or bulk virtual elements in the absence of curved boundaries, see for instance [1]. In the context of bulk- or bulk-surface virtual elements in the presence of curved boundaries, our analysis requires full H^2 -regularity of the exact solution on the polygonal domain. For this reason we need to consider, alongside the inverse-lifted exact solution $u^{-\ell}$, the alternative approximation $\tilde{u}|_{\Omega_h}$, that is the restriction to Ω_h of the Sobolev extension \tilde{u} of the exact solution u . Hence, we present the following variant of Lemma 3.*

Lemma 4 (Geometric error of Sobolev extension). *If $0 < \gamma < 1$, there exist $C > 0$ and $C_\gamma > 0$ such that*

$$\|\tilde{u} - u^{-\ell}\|_{L^2(\Omega_h)} \leq Ch^2 \|u\|_{H^{1+3/4}(\Omega)}, \quad \forall u \in H^{1+3/4}(\Omega); \quad (33)$$

$$|\tilde{u} - u^{-\ell}|_{H^1(\Omega_h)} \leq Ch^{3/2} \|u\|_{H^2(\Omega)} + C_\gamma h^{1/2+2\gamma} \|u\|_{H^{2+\gamma}(\Omega)}, \quad \forall u \in H^{2+\gamma}(\Omega). \quad (34)$$

Proof. By using (A.14), (A.15) with $\gamma = \frac{3}{4}$, (11) and (14) we have that

$$\begin{aligned} \|\tilde{u} - u^{-\ell}\|_{L^2(\Omega_h)} &= \|\tilde{u} - \tilde{u} \circ G\|_{L^2(\Omega_h)} \leq C \|\tilde{u}\|_{H^{1+3/4}(\Omega_h)} \|(Id - G)^{3/4}\|_{L^2(\Omega_h)} \\ &= C \|u\|_{H^{1+3/4}(\Omega)} \|(Id - G)^{3/4}\|_{L^2(\Omega_B)} \leq C \|u\|_{H^{1+3/4}(\Omega)} |\Omega_B|^{1/2} \|Id - G\|_{L^\infty(\Omega_B)}^{3/4} \\ &\leq Ch^{1/2} h^{3/2} \|u\|_{H^{1+3/4}(\Omega)} = Ch^2 \|u\|_{H^{1+3/4}(\Omega)}, \end{aligned} \quad (35)$$

which proves (33). Notice that, in the last line of (35), the $h^{1/2}$ term is the effect of the Sobolev extension being exact except that on the discrete narrow band Ω_B , while the $h^{3/2}$ terms is the approximation accuracy, which is intuitively justified by the Sobolev index $1 + 3/4$ being larger than the exponent $3/2$. Using (A.10), (A.14), (12) and (14) we have that

$$\begin{aligned} |\tilde{u} - u^{-\ell}|_{H^1(\Omega_h)} &= \|\nabla \tilde{u} - (JG^T \nabla \tilde{u}) \circ G\|_{L^2(\Omega_h)} \\ &\leq \|(Id - JG^T \circ G)\|_{L^\infty(\Omega_h)} \|\nabla \tilde{u}\|_{L^2(\Omega_B)} + \|JG^T \circ G\|_{L^\infty(\Omega_h)} \|\nabla \tilde{u} - \nabla \tilde{u} \circ G\|_{L^2(\Omega_h)} \\ &\leq Ch \|\nabla \tilde{u}\|_{L^2(\Omega_B)} + C \|\nabla \tilde{u} - \nabla \tilde{u} \circ G\|_{L^2(\Omega_h)} \leq Ch^{3/2} \|u\|_{H^2(\Omega)} + C \|\nabla \tilde{u} - \nabla \tilde{u} \circ G\|_{L^2(\Omega_h)}. \end{aligned} \quad (36)$$

Since $\tilde{u} \in H^{2+\gamma}(\Omega_h)$, then $\nabla \tilde{u} \in H^{1+\gamma}(\Omega_h)$. Hence, by reasoning as in (35) we have that

$$\|\nabla \tilde{u} - \nabla \tilde{u} \circ G\|_{L^2(\Omega_h)} \leq C_\gamma h^{1/2+2\gamma} \|u\|_{H^{2+\gamma}(\Omega)}. \quad (37)$$

By substituting (37) into (36) we get the desired estimate. \square

3.3 Virtual element space in the bulk

In this section we define virtual element spaces on polygons and polygonal domains by following [7]. Let E be a polygon in \mathbb{R}^2 . A preliminary virtual element space on E is given by

$$\tilde{\mathcal{V}}(E) := \left\{ v \in H^1(E) \cap \mathcal{C}^0(E) \mid v|_e \in \mathbb{P}_1(e), \forall e \in \text{edges}(E) \wedge \Delta v \in \mathbb{P}_1(E) \right\}, \quad (38)$$

where $\mathbb{P}_1(E)$ is the space of linear polynomials on the polygon E . The functions in $\mathbb{V}(E)$ are not known in closed form, but we are able to use them in a spatially discrete method, hence the name *virtual*. Let us consider the elliptic projection $\Pi_E^\nabla : \tilde{\mathbb{V}}(E) \rightarrow \mathbb{P}_1(E)$ defined by

$$\begin{cases} \int_E \nabla(v - \Pi_E^\nabla v) \cdot \nabla p_1 = 0, & \forall p_1 \in \mathbb{P}_1(E); \\ \int_{\partial E} (v - \Pi_E^\nabla v) = 0. \end{cases} \quad (39)$$

Using Green's formula, it is easy to see that the operator Π_E^∇ is computable, see [3] for the details. The so-called *enhanced virtual element space* in two dimensions is now defined as follows:

$$\mathbb{V}(E) := \left\{ v \in \tilde{\mathbb{V}}(E) \mid \int_E v p_1 = \int_E (\Pi_E^\nabla v) p_1, \forall p_1 \in \mathbb{P}_1(E) \right\}. \quad (40)$$

The practical usability of the space $\mathbb{V}(E)$ stems from the following result.

Proposition 1 (Degrees of freedom). *Let $n \in \mathbb{N}$. If E is a polygon with n vertices \mathbf{x}_i , $i = 1, \dots, n$, then $\dim(\mathbb{V}(E)) = n$ and each function $v \in \mathbb{V}(E)$ is uniquely defined by the nodal values $v(\mathbf{x}_i)$, $i = 1, \dots, n$. Hence, the nodal values constitute a set of degrees of freedom.*

Proof. See [3]. □

For $s = 1, 2$ we define the broken bulk Sobolev seminorms as $|u|_{s, \Omega, h} := \sum_{E \in \mathcal{E}_h} |u|_{H^s(E)}$. The approximation properties of the space $\mathbb{V}(E)$ are given by the following result.

Proposition 2 (Projection error on $\mathbb{P}_1(E)$). *For all $E \in \mathcal{E}_h$, $s \in \{1, 2\}$ and $w \in H^s(E)$ there exists $w_\pi \in \mathbb{P}_1(E)$ such that*

$$\|w - w_\pi\|_{L^2(E)} + h_E |w - w_\pi|_{H^1(E)} \leq Ch_E^s |w|_{H^s(E)}, \quad (41)$$

where C is a constant that depends only on γ_1 .

Proof. See [3]. □

Remark 4 (Regularity of $\mathbb{V}(E)$ functions). *If E is a convex polygon, from the properties of the Poisson problem on convex Lipschitz domains, it holds that $\mathbb{V}(E) \subset H^2(E)$, see for instance [40]. Otherwise, if E is non-convex, we may only assert that $\mathbb{V}(E) \subset H^{1+\varepsilon}(E)$ for $0 \leq \varepsilon < 1/2$, see [40]. In either case, $\mathbb{V}(E) \subset \mathcal{C}^0(E)$, see Theorem A5. We will account for this regularity issue in devising a numerical method with optimal convergence.*

The discontinuous- and continuous bulk virtual element spaces are defined by pasting local spaces:

$$\mathbb{V}_{\Omega, h} := \{v : \Omega_h \rightarrow \mathbb{R} \mid v|_E \in \mathbb{V}(E), \forall E \in \mathcal{E}_h\}; \quad \mathbb{V}_\Omega := \mathbb{V}_{\Omega, h} \cap \mathcal{C}^0(\Omega_h). \quad (42)$$

Thanks to Remark 4, the only source of discontinuity in $\mathbb{V}_{\Omega, h}$ are jumps across edges. In \mathbb{V}_Ω we consider the Lagrange basis

$$\varphi_i \in \mathbb{V}_\Omega, \quad i = 1, \dots, N, \quad (43)$$

where, for each $i = 1, \dots, N$, φ_i is the unique \mathbb{V}_Ω function such that $\varphi_i(\mathbf{x}_j) = \delta_{ij}$, $\forall j = 1, \dots, N$, with δ_{ij} being the Kronecker symbol. The set $\{\varphi_i, i = 1, \dots, N\}$ is a basis of \mathbb{V}_Ω thanks to Proposition 1.

3.4 Approximation of bilinear forms in the bulk

In order to derive a spatially discrete formulation of the weak continuous problems (4) and (5) we need suitable approximate bilinear forms in the bulk Ω_h . We will follow [3, 5]. In the remainder of this section, let E be an element of Ω_h . The *stabilizing form* $S_E : \mathbb{V}(E) \times \mathbb{V}(E) \rightarrow \mathbb{R}$, is defined by

$$S_E(v, w) := \sum_{P \in \text{vertices}(E)} v(P)w(P), \quad \forall v, w \in \mathbb{V}(E). \quad (44)$$

The L^2 projector $\Pi_E^0 : \mathbb{V}(E) \rightarrow \mathbb{P}_1(E)$ is defined as follows: for $w \in \mathbb{V}(E)$:

$$\int_E (w - \Pi_E^0 w) p_1 = 0, \quad \forall p_1 \in \mathbb{P}_1(E). \quad (45)$$

As shown in [3], Π_E^0 is computable because $\Pi_E^0 = \Pi_E^\nabla$. Even if Π_E^0 is not a new projector, the presentation and the analysis of the method benefit from the usage of the equivalent definition (45). Moreover, since $\Pi_E^0 = \Pi_E^\nabla$, the boundedness property of projection operators in Hilbert spaces translates to

$$\|\Pi_E^0 w\|_{L^2(E)} \leq \|w\|_{L^2(E)} \quad \text{and} \quad |\Pi_E^0 w|_{H^1(E)} \leq |w|_{H^1(E)}. \quad (46)$$

We are now ready to introduce the approximate L^2 bilinear form $m_E : \mathbb{V}(E) \times \mathbb{V}(E) \rightarrow \mathbb{R}$, defined as follows:

$$m_E(v, w) := \int_E (\Pi_E^0 v)(\Pi_E^0 w) + \text{area}(E) S_E(v - \Pi_E^0 v, w - \Pi_E^0 w), \quad (47)$$

for all $v, w \in \mathbb{V}(E)$. The approximate gradient-gradient bilinear form $a_E : \mathbb{V}(E) \times \mathbb{V}(E) \rightarrow \mathbb{R}$ is defined by

$$a_E(v, w) := \int_E (\nabla \Pi_E^\nabla v) \cdot (\nabla \Pi_E^\nabla w) + h_E S_E(v - \Pi_E^\nabla v, w - \Pi_E^\nabla w), \quad (48)$$

for all $v, w \in \mathbb{V}(E)$, where h_E is the diameter of E . The following result easily follows from the construction of the bilinear forms of a_h and m_h .

Proposition 3 (Stability and consistency). *The bilinear forms a_h and m_h are consistent, i.e. for all $v \in \mathbb{V}(E)$ and $p \in \mathbb{P}_1(E)$*

$$a_E(v, p) = \int_E \nabla v \cdot \nabla p; \quad \text{and} \quad m_E(v, p) = \int_E vp. \quad (49)$$

The bilinear forms a_h and m_h are stable, meaning that there exists two constants $0 < \alpha_ < \alpha^*$ depending on γ_2 such that, for all $v \in \mathbb{V}(E)$*

$$\alpha_* \int_E \nabla v \cdot \nabla v \leq a_E(v, v) \leq \alpha^* \int_E \nabla v \cdot \nabla v; \quad (50)$$

$$\alpha_* \int_E v^2 \leq m_E(v, v) \leq \alpha^* \int_E v^2. \quad (51)$$

Proof. See [5]. □

We observe from (50) and (51) that the error in the approximate bilinear forms a_E and m_E is not a function of the meshsize h , see also [5]. Nevertheless, we will show that the method retains optimal convergence thanks to the consistency properties (49). The global bilinear forms are defined by pasting the corresponding local bilinear forms as follows:

$$m_h(v, w) := \sum_{E \in \mathcal{E}_h} m_E(v|_E, w|_E), \quad \forall v, w \in \mathbb{V}_\Omega; \quad (52)$$

$$a_h(v, w) := \sum_{E \in \mathcal{E}_h} a_E(v|_E, w|_E), \quad \forall v, w \in \mathbb{V}_\Omega. \quad (53)$$

A consequence of Proposition 3 is that $m_h : \mathbb{V}_\Omega \times \mathbb{V}_\Omega \rightarrow \mathbb{R}$ is positive definite, while $a_h : \mathbb{V}_\Omega \times \mathbb{V}_\Omega \rightarrow \mathbb{R}$ is positive semi-definite.

3.5 Approximation of the load term in the bulk

The approximate bilinear forms presented in the previous section are not sufficient to discretise load terms like $\int_\Omega f \varphi$, because f is not in the space \mathbb{V}_Ω . We resolve this issue by combining approaches in [1] and [28, 29]. From [1] we take the usage of the projection operator Π^∇ , while from [28, 29] we take the usage of the Lagrange interpolant. In the context of virtual elements, the Lagrange interpolant is defined as follows.

Definition 3 (Virtual Lagrange Interpolant). *Given an element-wise continuous function $f : \Omega_h \rightarrow \mathbb{R}$, $f|_E \in \mathcal{C}(E)$ for all $E \in \mathcal{E}_h$, the virtual Lagrange interpolant $I_\Omega f$ of f is the unique $\mathbb{V}_{\Omega, h}$ function such that*

$$I_\Omega f|_E(\mathbf{x}_i) = f(\mathbf{x}_i), \quad \forall i : \mathbf{x}_i \in \text{nodes}(E), \quad \forall E \in \mathcal{E}_h. \quad (54)$$

In particular, if $f \in \mathcal{C}(\Omega_h)$, then $I_\Omega f$ is the unique \mathbb{V}_Ω function such that

$$I_\Omega f(\mathbf{x}_i) = f(\mathbf{x}_i), \quad \forall i = 1, \dots, N. \quad (55)$$

The following result provides an estimate of the interpolation error in the bulk.

Proposition 4 (Interpolation error in the bulk). *If $w : \Omega_h \rightarrow \mathbb{R}$ is such that $w_E \in H^2(E)$ for all $E \in \mathcal{E}_h$, then the interpolant $I_\Omega(w)$ fulfils*

$$\|w - I_\Omega(w)\|_{L^2(\Omega_h)} + h|w - I_\Omega(w)|_{1, \Omega, h} \leq Ch^2|w|_{2, \Omega, h}, \quad (56)$$

where $C > 0$ depends only on γ_1 .

Proof. See [3]. □

Unlike projection operators, we may not assert that the interpolant I_Ω is bounded in $L^2(\Omega_h)$. However from (56) we have the *quasi-boundedness* of I_Ω in $L^2(\Omega_h)$:

$$\|I_\Omega(w)\|_{L^2(\Omega_h)} \leq \|w\|_{L^2(\Omega_h)} + Ch^2|w|_{2, \Omega, h}, \quad (57)$$

where $C > 0$ depends only on γ_1 .

3.6 Finite element space and discrete load term on the curve

Let $F \in \mathcal{F}_h$ be an edge of the approximated curve Γ_h . The local finite element space on F is the space $\mathbb{P}_1(F)$ of linear polynomials on F . The global finite element space on Γ_h is defined by

$$\mathbb{V}_\Gamma := \left\{ v \in \mathcal{C}^0(\Gamma_h) \mid v|_F \in \mathbb{P}_1(F), \text{ for all } F \in \mathcal{F}_h \right\}, \quad (58)$$

i.e. the space of piecewise linear functions on the approximated curve Γ_h . On \mathbb{V}_Γ we consider the Lagrange basis

$$\psi_k \in \mathbb{V}_\Gamma, \quad k = 1, \dots, M, \quad (59)$$

where, for each $k = 1, \dots, M$, ψ_k is the unique \mathbb{V}_Γ function such that

$$\psi_k(\mathbf{x}_l) = \delta_{kl}, \quad \forall l = 1, \dots, M. \quad (60)$$

It is easy to see that the Lagrange basis functions of \mathbb{V}_Ω and \mathbb{V}_Γ , defined in (43) and (59) respectively, fulfil the following relation:

$$\varphi_{k|\Gamma_h} = \psi_k, \quad \forall k = 1, \dots, M, \quad (61)$$

i.e. the Lagrange basis functions of \mathbb{V}_Γ are the restrictions of the first M Lagrange basis functions of \mathbb{V}_Ω on the piecewise linear curve Γ_h . Before introducing the spatially discrete formulations, we are left to treat terms like $\int_\Gamma g \varphi$, since g is not in the boundary finite element space \mathbb{V}_Γ .

Definition 4 (Surface Lagrange interpolant). *If $g : \Gamma_h \rightarrow \mathbb{R}$ is a continuous function, the Lagrange interpolant $I_\Gamma(g)$ of g is the unique \mathbb{V}_Γ function such that*

$$I_\Gamma(g)(\mathbf{x}_i) = g(\mathbf{x}_i), \quad \forall i = 1, \dots, M. \quad (62)$$

We consider the following broken surface Sobolev norm

$$|v|_{2,\Gamma,h} := \sum_{F \in \mathcal{F}_h} |V|_F|_{H^2(F)}.$$

The following are basic properties of Lagrange interpolation.

Lemma 5 (Properties of Lagrange interpolation on the surface). *Let $v \in \mathcal{C}^0(\Gamma_h)$ such that, for every $F \in \mathcal{F}_h$, $v|_F \in H^2(F)$. Then*

$$\|v - I_\Gamma(v)\|_{L^2(\Gamma_h)} + h|v - I_\Gamma(v)|_{H^1(\Gamma_h)} \leq Ch^2|v|_{2,\Gamma,h}. \quad (63)$$

The surface Lagrange interpolant is monotonic, that is if $v \leq w$ then:

$$I_\Gamma(v) \leq I_\Gamma(w). \quad (64)$$

Proof. See [20] for (63), while (64) follows by definition. \square

3.7 The spatially discrete formulations

We are now ready to introduce the *bulk-surface virtual element discretisation* of the weak problems (4) and (5).

3.7.1 The elliptic problem

The discrete counterpart of the elliptic problem (4) is: find $U \in \mathbb{V}_\Omega$ and $V \in \mathbb{V}_\Gamma$ such that

$$\begin{cases} a_h(U, \varphi) + m_h(U, \varphi) + \int_{\Gamma_h} (\alpha U - \beta V) \varphi = m_h(I_\Omega(f), \varphi); \\ \int_{\Gamma_h} \nabla_{\Gamma_h} V \cdot \nabla_{\Gamma_h} \psi + \int_{\Gamma_h} (-\alpha U + (\beta + 1)V) \psi = \int_{\Gamma_h} I_\Gamma(g) \psi, \end{cases} \quad (65)$$

for all $\varphi \in \mathbb{V}_\Omega$ and $\psi \in \mathbb{V}_\Gamma$. We express the spatially discrete solution (U, V) in the Lagrange bases as follows:

$$U(\mathbf{x}) = \sum_{i=1}^N \xi_i \varphi_i(\mathbf{x}), \quad \mathbf{x} \in \Omega_h; \quad \text{and} \quad V(\mathbf{x}) = \sum_{k=1}^M \eta_k \psi_k(\mathbf{x}), \quad \mathbf{x} \in \Gamma_h. \quad (66)$$

Hence, problem (65) is equivalent to: find $\boldsymbol{\xi} := (\xi_1, \dots, \xi_N)^T \in \mathbb{R}^N$ and $\boldsymbol{\eta} := (\eta_1, \dots, \eta_M)^T \in \mathbb{R}^M$ such that

$$\begin{cases} \sum_{i=1}^N \xi_i a_h(\varphi_i, \varphi_j) + \sum_{i=1}^N \xi_i m_h(\varphi_i, \varphi_j) + \alpha \sum_{k=1}^M \xi_k \int_{\Gamma_h} \varphi_k \varphi_l \\ \quad - \beta \sum_{k=1}^M \eta_k \int_{\Gamma_h} \psi_k \varphi_l = \sum_{i=1}^N f(\mathbf{x}_i) m_h(\varphi_i, \varphi_j); \\ \sum_{k=1}^M \eta_k \int_{\Gamma_h} \nabla_{\Gamma_h} \psi_k \cdot \nabla_{\Gamma_h} \psi_l - \alpha \sum_{k=1}^M \xi_k \int_{\Gamma_h} \varphi_k \psi_l \\ \quad + (\beta + 1) \sum_{k=1}^M \eta_k \int_{\Gamma_h} \psi_k \psi_l = \sum_{k=1}^M g(\mathbf{x}_k) \int_{\Gamma_h} \psi_k \psi_l, \end{cases} \quad (67)$$

for all $j = 1, \dots, N$ and $l = 1, \dots, M$. We consider the matrices $A_\Omega = (a_{i,j}^\Omega) \in \mathbb{R}^{N \times N}$, $M_\Omega = (m_{i,j}^\Omega) \in \mathbb{R}^{N \times N}$, $A_\Gamma = (a_{k,l}^\Gamma) \in \mathbb{R}^{M \times M}$, $M_\Gamma = (m_{k,l}^\Gamma) \in \mathbb{R}^{M \times M}$ defined as follows:

$$a_{i,j}^\Omega := a_h(\varphi_i, \varphi_j), \quad i, j = 1, \dots, N; \quad (68)$$

$$m_{i,j}^\Omega := m_h(\varphi_i, \varphi_j), \quad i, j = 1, \dots, N; \quad (69)$$

$$a_{k,l}^\Gamma := \int_{\Gamma_h} \nabla_{\Gamma_h} \psi_k \cdot \nabla_{\Gamma_h} \psi_l, \quad k, l = 1, \dots, M; \quad (70)$$

$$m_{k,l}^\Gamma := \int_{\Gamma_h} \psi_k \psi_l, \quad k, l = 1, \dots, M. \quad (71)$$

Moreover, we consider the column vectors $\mathbf{f} \in \mathbb{R}^N$ and $\mathbf{g} \in \mathbb{R}^M$ defined by

$$\mathbf{f} := \begin{bmatrix} f(\mathbf{x}_1) \\ \vdots \\ f(\mathbf{x}_N) \end{bmatrix} \quad \text{and} \quad \mathbf{g} := \begin{bmatrix} g(\mathbf{x}_1) \\ \vdots \\ g(\mathbf{x}_M) \end{bmatrix}. \quad (72)$$

By using (61) we can now rewrite the discrete formulation (67) in matrix-vector form as a block $(N + M) \times (N + M)$ linear algebraic system:

$$\begin{cases} A_\Omega \boldsymbol{\xi} + M_\Omega \boldsymbol{\xi} + \alpha R M_\Gamma R^T \boldsymbol{\xi} - \beta R M_\Gamma \boldsymbol{\eta} = M_\Omega \mathbf{f}; \\ A_\Gamma \boldsymbol{\eta} - \alpha M_\Gamma R^T \boldsymbol{\xi} + (\beta + 1) M_\Gamma \boldsymbol{\eta} = M_\Gamma \mathbf{g}. \end{cases} \quad (73)$$

In compact form, the linear system (73) reads

$$\begin{bmatrix} A_\Omega + M_\Omega + \alpha R M_\Gamma R^T & -\beta R M_\Gamma \\ -\alpha M_\Gamma R^T & A_\Gamma + (\beta + 1) M_\Gamma \end{bmatrix} \begin{bmatrix} \boldsymbol{\xi} \\ \boldsymbol{\eta} \end{bmatrix} = \begin{bmatrix} M_\Omega \mathbf{f} \\ M_\Gamma \mathbf{g} \end{bmatrix}, \quad (74)$$

which is uniquely solvable thanks to the following theorem.

Theorem 2 (Positive definiteness of the discrete elliptic problem). *The matrix*

$$\mathbf{A} := \begin{bmatrix} A_\Omega + M_\Omega + \alpha R M_\Gamma R^T & -\beta R M_\Gamma \\ -\alpha M_\Gamma R^T & A_\Gamma + (\beta + 1) M_\Gamma \end{bmatrix} \quad (75)$$

is positive definite.

Proof. Let $\boldsymbol{\xi} \in \mathbb{R}^N$, $\boldsymbol{\xi} \neq \mathbf{0}$ and $\boldsymbol{\eta} \in \mathbb{R}^M$, $\boldsymbol{\eta} \neq \mathbf{0}$. Let us denote $\boldsymbol{\xi}_\Gamma := R^T \boldsymbol{\xi}$. From (68), (69), the positive semi-definiteness of a_h and the positive definiteness of m_h we have that A_Ω is positive semi-definite and M_Ω is positive definite. Similarly, from (70) and (71), we have that A_Γ is positive semi-definite and M_Γ is positive definite. To prove that \mathbf{A} is positive definite, we observe that

$$\begin{aligned} [\boldsymbol{\xi}^T, \boldsymbol{\eta}^T] \mathbf{A} \begin{bmatrix} \boldsymbol{\xi} \\ \boldsymbol{\eta} \end{bmatrix} &= \boldsymbol{\xi}^T (A_\Omega + M_\Omega + \alpha R M_\Gamma R^T) \boldsymbol{\xi} - \beta \boldsymbol{\xi}_\Gamma^T M_\Gamma \boldsymbol{\eta} \\ &\quad - \alpha \boldsymbol{\eta} M_\Gamma \boldsymbol{\xi}_\Gamma + \boldsymbol{\eta}^T (A_\Gamma + (\beta + 1) M_\Gamma) \boldsymbol{\eta}. \end{aligned} \quad (76)$$

From Cauchy-Schwarz inequality, we have the following inequality

$$\begin{aligned} [\boldsymbol{\xi}^T, \boldsymbol{\eta}^T] \mathbf{A} \begin{bmatrix} \boldsymbol{\xi} \\ \boldsymbol{\eta} \end{bmatrix} &\geq \boldsymbol{\xi}^T A_\Omega \boldsymbol{\xi} + \boldsymbol{\xi}^T M_\Omega \boldsymbol{\xi} + \alpha \boldsymbol{\xi}_\Gamma^T M_\Gamma \boldsymbol{\xi}_\Gamma - \beta \sqrt{\boldsymbol{\xi}_\Gamma^T M_\Gamma \boldsymbol{\xi}_\Gamma} \sqrt{\boldsymbol{\eta}^T M_\Gamma \boldsymbol{\eta}} \\ &\quad - \alpha \sqrt{\boldsymbol{\eta}^T M_\Gamma \boldsymbol{\eta}} \sqrt{\boldsymbol{\xi}_\Gamma^T M_\Gamma \boldsymbol{\xi}_\Gamma} + \boldsymbol{\eta}^T A_\Gamma \boldsymbol{\eta} + (\beta + 1) \boldsymbol{\eta}^T M_\Gamma \boldsymbol{\eta}. \end{aligned} \quad (77)$$

From Young's inequality, it follows then that

$$[\boldsymbol{\xi}^T, \boldsymbol{\eta}^T] \mathbf{A} \begin{bmatrix} \boldsymbol{\xi} \\ \boldsymbol{\eta} \end{bmatrix} \geq \boldsymbol{\xi}^T A_\Omega \boldsymbol{\xi} + \boldsymbol{\xi}^T M_\Omega \boldsymbol{\xi} + \boldsymbol{\eta}^T A_\Gamma \boldsymbol{\eta} + \frac{\alpha}{2} \boldsymbol{\xi}_\Gamma^T M_\Gamma \boldsymbol{\xi}_\Gamma + \left(1 + \frac{\beta}{2}\right) \boldsymbol{\eta}^T M_\Gamma \boldsymbol{\eta} > 0. \quad (78)$$

□

3.7.2 The parabolic problem

The spatial discretisation of the parabolic problem (5) is: find $U \in L^2([0, T]; \mathbb{V}_\Omega)$ and $V \in L^2([0, T]; \mathbb{V}_\Gamma)$ such that

$$\begin{cases} m_h \left(\frac{\partial U}{\partial t}, \varphi \right) + d_u a_h(U, \varphi) = m_h(\Pi^0 I_\Omega(q(\Pi^0 U)), \varphi) + \int_{\Gamma_h} I_\Gamma(s(U, V)) \varphi; \\ \int_{\Gamma_h} \frac{\partial V}{\partial t} \psi + d_v \int_{\Gamma} \nabla_{\Gamma_h} V \cdot \nabla_{\Gamma_h} \psi + \int_{\Gamma_h} I_\Gamma(s(U, V)) \psi = \int_{\Gamma_h} I_\Gamma(r(U, V)) \psi, \end{cases} \quad (79)$$

for all $U \in L^2([0, T]; \mathbb{V}_\Omega)$ and $V \in L^2([0, T]; \mathbb{V}_\Gamma)$. The discrete initial conditions are prescribed as follows

$$U_0 = I_\Omega(u_0), \quad \text{and} \quad V_0 = I_\Gamma(v_0). \quad (80)$$

Remark 5 (Special cases). *If every element $E \in \mathcal{E}_h$ is convex or f is linear, optimal convergence is retained by replacing the term $m_h(\Pi^0 I_\Omega(q(\Pi^0 U)), \varphi)$ with $m_h(I_\Omega(q(U)), \varphi)$, i.e by removing the projection operator Π^0 . By expressing the time-dependent semi-discrete solution (U, V) in the Lagrange basis as follows*

$$U(\mathbf{x}, t) = \sum_{i=1}^N \xi_i(t) \varphi_i(\mathbf{x}), \quad \mathbf{x} \in \Omega_h; \quad (81)$$

and

$$V(\mathbf{x}, t) = \sum_{k=1}^M \eta_k(t) \psi_k(\mathbf{x}), \quad \mathbf{x} \in \Gamma_h, \quad (82)$$

the fully discrete problem can be written in matrix-vector form as an $(M + N) \times (M + N)$ nonlinear ODE system of the form:

$$\begin{cases} M_\Omega \dot{\boldsymbol{\xi}}(t) + K_\Omega \boldsymbol{\xi}(t) = M_\Omega q(\boldsymbol{\xi}(t)) + R M_\Gamma h(R^T \boldsymbol{\xi}(t), \boldsymbol{\eta}(t)); \\ M_\Gamma \dot{\boldsymbol{\eta}}(t) + K_\Gamma \boldsymbol{\eta}(t) = -M_\Gamma h(R^T \boldsymbol{\xi}(t), \boldsymbol{\eta}(t)) + M_\Gamma r(R^T \boldsymbol{\xi}(t), \boldsymbol{\eta}(t)). \end{cases} \quad (83)$$

Remark 6 (Implementation). *Thanks to the reduction matrix R , we are able to implement the spatially discrete problems (73) and (83) by using only two kinds of mass matrix (M_Ω and M_Γ), two kinds of stiffness matrix (A_Ω and A_Γ) and R itself. In previous works on BSFEM as illustrated in [35], five kinds of mass matrix were used to evaluate the integrals appearing in the spatially discrete formulation. We stress once again that, since the pre-existing BSFEM is a special case of the proposed BSVEM, this work provides, as a by-product, an optimised matrix implementation of the BSFEM.*

4 Stability and convergence analysis

The spatially discrete parabolic problem (79) fulfils the following stability estimates.

Lemma 6 (Stability estimates for the spatially discrete parabolic problem (79)). *There exists $C > 0$ depending on q, r, s and Ω such that*

$$\begin{aligned} \sup_{t \in [0, T]} \left(\|U\|_{L^2(\Omega_h)}^2 + \|V\|_{L^2(\Gamma_h)}^2 \right) + \int_0^T \left(|U|_{H^1(\Omega_h)}^2 + |V|_{H^1(\Gamma_h)}^2 \right) \\ \leq C \left(1 + \|U_0\|_{L^2(\Omega_h)}^2 + \|V_0\|_{L^2(\Gamma_h)}^2 \right) \exp(CT); \end{aligned} \quad (84)$$

$$\begin{aligned} \sup_{t \in [0, T]} \left(|U|_{H^1(\Omega_h)}^2 + |V|_{H^1(\Gamma_h)}^2 \right) + \int_0^T \left(\|\dot{U}\|_{L^2(\Omega_h)}^2 + \|\dot{V}\|_{L^2(\Gamma_h)}^2 \right) \\ \leq C \left(1 + \|U_0\|_{H^1(\Omega_h)}^2 + \|V_0\|_{H^1(\Gamma_h)}^2 \right) \exp(CT). \end{aligned} \quad (85)$$

Proof. The proof relies on standard energy techniques. By choosing $\varphi = U$ and $\psi = V$ in (79), using the Lipschitz continuity of q, r, s , the Young's inequality and summing over the equations we have

$$\begin{aligned} \frac{1}{2} \frac{d}{dt} \left(m_h(U, U) + \|V\|_{L^2(\Gamma_h)}^2 \right) + d_u a_h(U, U) + d_v |V|_{H^1(\Gamma_h)}^2 \\ \leq C \left(1 + \|U\|_{L^2(\Omega_h)}^2 + \|V\|_{L^2(\Gamma_h)}^2 \right) + c \|U|_{\Gamma_h}\|_{L^2(\Gamma_h)}^2, \end{aligned} \quad (86)$$

where $c > 0$ is arbitrarily small, thanks to the Young's inequality. By applying (26), (A.11) and (50) to the last term in (86) we can choose c such that we have

$$\begin{aligned} \frac{1}{2} \frac{d}{dt} \left(m_h(U, U) + \|V\|_{L^2(\Gamma_h)}^2 \right) + d_u a_h(U, U) + d_v |V|_{H^1(\Gamma_h)}^2 \\ \leq C \left(1 + \|U\|_{L^2(\Omega_h)}^2 + \|V\|_{L^2(\Gamma_h)}^2 \right) + \frac{d_u}{2} a_h(U, U). \end{aligned} \quad (87)$$

By using (51) into (87) we have

$$\begin{aligned} \frac{1}{2} \frac{d}{dt} \left(m_h(U, U) + \|V\|_{L^2(\Gamma_h)}^2 \right) \leq C \left(m_h(U, U) + \|V\|_{L^2(\Omega_h)}^2 \right) \\ + C - \frac{d_u}{2} a_h(U, U) - d_v |V|_{H^1(\Gamma_h)}^2. \end{aligned} \quad (88)$$

An application of Grönwall's lemma to (88) yields

$$\begin{aligned} \sup_{t \in [0, T]} \left(m_h(U, U) + \|V\|_{L^2(\Gamma_h)}^2 \right) \leq \left(1 + m_h(U_0, U_0) + \|V_0\|_{L^2(\Gamma_h)}^2 \right) \exp(CT) - 1 \\ - \int_0^T \left(\frac{d_u}{2} a_h(U, U) + d_v |V|_{H^1(\Gamma_h)}^2 \right) \exp\{C(T-t)\} dt, \end{aligned} \quad (89)$$

which yields (84) after an application of (26). Similarly, by choosing $\varphi = \dot{U}$ and $\psi = \dot{V}$ in (79) and summing over the equations we have

$$\begin{aligned} m_h(\dot{U}, \dot{U}) + \|\dot{V}\|_{L^2(\Gamma_h)}^2 + \frac{1}{2} \frac{d}{dt} \left(d_u a_h(U, U) + d_v |V|_{H^1(\Gamma_h)}^2 \right) \\ \leq C \left(1 + \|U\|_{L^2(\Omega_h)}^2 + \|V\|_{L^2(\Gamma_h)}^2 \right) + C a_h(U, U) + \frac{1}{2} \left(m_h(\dot{U}, \dot{U}) + \|\dot{V}\|_{L^2(\Gamma_h)}^2 \right), \end{aligned} \quad (90)$$

where we have exploited the Lipschitz continuity of q , r , s and the Young's inequality and (51). From (90) we immediately get

$$\begin{aligned} \frac{1}{2} \left(m_h(\dot{U}, \dot{U}) + \|\dot{V}\|_{L^2(\Gamma_h)}^2 \right) + \frac{1}{2} \frac{d}{dt} \left(d_u a_h(U, U) + d_v |V|_{H^1(\Gamma_h)}^2 \right) \\ \leq C \left(a_h(U, U) + |V|_{H^1(\Gamma_h)}^2 \right) + C \left(1 + \|U\|_{L^2(\Omega_h)}^2 + \|V\|_{L^2(\Gamma_h)}^2 \right). \end{aligned} \quad (91)$$

By applying Grönwall's lemma and then using (50)-(51) we obtain (85). \square

To derive error estimates for the spatially discrete solution we need suitable bulk- and surface Ritz projections. The surface Ritz projection is taken from [26], while the bulk Ritz projection is tailor-made.

Definition 5 (Surface Ritz projection). *The surface Ritz projection of a function $v \in H^1(\Gamma)$ is the unique function $\mathcal{R}v \in \mathbb{V}_\Gamma$ such that*

$$\int_{\Gamma_h} \nabla_{\Gamma_h} \mathcal{R}v \cdot \nabla_{\Gamma_h} \psi = \int_{\Gamma} \nabla_{\Gamma} v \cdot \nabla_{\Gamma} \psi, \quad \forall \psi \in \mathbb{V}_\Gamma, \quad (92)$$

$$\int_{\Gamma_h} \mathcal{R}v = \int_{\Gamma} v. \quad (93)$$

Theorem 3 (Error bounds for the surface Ritz projection). *The surface Ritz projection fulfils the optimal a priori error bound*

$$\|v - (\mathcal{R}v)^\ell\|_{L^2(\Gamma)} + h\|v - (\mathcal{R}v)^\ell\|_{H^1(\Gamma)} \leq Ch^2\|v\|_{H^2(\Gamma)}, \quad (94)$$

where $C > 0$ depends only on Γ and ℓ is the lifting.

Proof. See [26]. □

We now define a suitable Ritz projection in the bulk.

Definition 6 (Bulk Ritz projection). *The bulk Ritz projection of a function $u \in H^1(\Omega)$ is the unique function $\mathcal{R}u \in \mathbb{V}_\Omega$ such that*

$$a_h(\mathcal{R}u, \psi) = \int_{\Omega} \nabla u \cdot \nabla \psi^\ell, \quad \forall \psi \in \mathbb{V}_\Omega, \quad (95)$$

$$\mathcal{R}u|_{\Gamma_h} = I_\Gamma(u^{-\ell}), \quad (96)$$

where $-\ell$ is the inverse lifting.

In the following theorems we show that the bulk Ritz projection of a sufficiently regular function fulfils optimal a priori error bounds in $H^1(\Omega)$, $H^1(\Gamma)$, $L^2(\Gamma)$ and $L^2(\Omega)$ norms.

Theorem 4 ($H^1(\Omega)$ a priori error bound for the bulk Ritz projection). *For any $u \in H^{2+1/4}(\Omega)$ it holds that*

$$|u - (\mathcal{R}u)^\ell|_{H^1(\Omega)} \leq Ch\|u\|_{H^2(\Omega)} + Ch\|u\|_{H^{2+1/4}(\Omega)}, \quad (97)$$

where ℓ is the lifting.

Proof. We set $e_h := \mathcal{R}u - \tilde{u}$. From (29), (34), (41), (49), (50) and (95) we have

$$\begin{aligned} \alpha_* |e_h|_{H^1(\Omega_h)}^2 &\leq a_h(e_h, e_h) = a_h(\mathcal{R}u, e_h) - a_h(\tilde{u}, e_h) \\ &= \int_{\Omega} \nabla u \cdot \nabla e_h^\ell - \sum_{E \in \mathcal{E}_h} (a_E(\tilde{u}, e_h)) = \int_{\Omega} \nabla u \cdot \nabla e_h^\ell - \sum_{E \in \mathcal{E}_h} (a_E(\tilde{u} - \tilde{u}_\pi, e_h) + a_E(\tilde{u}_\pi, e_h)) \\ &= \int_{\Omega} \nabla u \cdot \nabla e_h^\ell - \int_{\Omega_h} \nabla \tilde{u} \cdot \nabla e_h - \sum_{E \in \mathcal{E}_h} a_E(\tilde{u} - \tilde{u}_\pi, e_h) \\ &= \int_{\Omega} \nabla u \cdot \nabla e_h^\ell - \int_{\Omega_h} \nabla u^{-\ell} \cdot \nabla e_h + \int_{\Omega_h} \nabla u^{-\ell} \cdot \nabla e_h - \int_{\Omega_h} \nabla \tilde{u} \cdot \nabla e_h - \sum_{E \in \mathcal{E}_h} a_E(\tilde{u} - \tilde{u}_\pi, e_h) \\ &\leq C \left(h\|u\|_{H^2(\Omega)} + h^{3/2}\|u\|_{H^2(\Omega)} + Ch\|u\|_{H^{2+1/4}(\Omega)} \right) |e_h|_{H^1(\Omega_h)}, \end{aligned}$$

which yields, for $h \leq h_0$

$$|e_h|_{H^1(\Omega_h)} \leq \left(Ch\|u\|_{H^2(\Omega)} + Ch\|u\|_{H^{2+1/4}(\Omega)} \right). \quad (98)$$

By using (26), (34) and (98) we get

$$\begin{aligned} |u - (\mathcal{R}u)^\ell|_{H^1(\Omega)} &\leq C|u^{-\ell} - \mathcal{R}u|_{H^1(\Omega_h)} \leq C(|u^{-\ell} - \tilde{u}|_{H^1(\Omega_h)} + |e_h|_{H^1(\Omega_h)}) \\ &\leq Ch\|u\|_{H^2(\Omega)} + Ch\|u\|_{H^{2+1/4}(\Omega)}. \end{aligned}$$

□

In order to prove the L^2 convergence care must be taken about inverse trace operators. A consequence of Theorem A3 is that, given $v \in H^1(\Gamma)$, there exists $v_B \in H^1(\Omega)$ such that $\text{Tr}(v_B) = v$ and $\|v_B\|_{H^1(\Omega)} \leq C\|v\|_{H^1(\Gamma)}$. However, for our purposes, we need the existence of a constant $C > 0$ such that the bounds $\|v_B\|_{L^2(\Omega)} \leq C\|v\|_{L^2(\Gamma)}$ and $|v_B|_{H^1(\Omega)} \leq C\|v\|_{H^1(\Gamma)}$ are simultaneously fulfilled, namely we need a L^2 -preserving inverse trace operator. In the following result we prove the existence of such an operator under special assumptions on the regularity of Γ .

Lemma 7 (L^2 -preserving inverse trace). *Assume the boundary Γ is \mathcal{C}^3 . Then, for any $v \in H^1(\Gamma)$ such that $\|v\|_{L^2(\Gamma)}$ is sufficiently small, there exists $v_B \in H^1(\Omega)$ such that*

$$\|v_B\|_{L^2(\Omega)} \leq C\|v\|_{L^2(\Gamma)}; \quad \text{and} \quad |v_B|_{H^1(\Omega)} \leq C\|v\|_{H^1(\Gamma)}. \quad (99)$$

Proof. With δ as defined in Theorem A1, we take $0 \leq \delta_0 \leq \delta$ and we define

$$v_B(\mathbf{x}) := \begin{cases} v(\mathbf{a}(\mathbf{x})) \left(1 + \frac{d(\mathbf{x})}{\delta_0}\right), & \text{if } \mathbf{x} \in U_{\delta_0}; \\ 0, & \text{if } \mathbf{x} \in \Omega \setminus U_{\delta_0}. \end{cases} \quad (100)$$

By using (A.9) we have

$$\begin{aligned} \int_{\Omega} v_B^2(\mathbf{x}) dx &= \int_{U_h} v_B^2(\mathbf{x}) dx = \int_{-\delta_0}^0 ds \int_{\Gamma_s} v^2(\mathbf{a}(\mathbf{x})) \left(1 + \frac{d(\mathbf{x})}{\delta_0}\right)^2 dx \\ &= \int_{-\delta_0}^0 \left(1 + \frac{s}{\delta_0}\right)^2 ds \int_{\Gamma_s} v^2(\mathbf{a}(\mathbf{x})) dx = \frac{\delta_0}{3} \int_{\Gamma_s} v^2(\mathbf{a}(\mathbf{x})) dx. \end{aligned} \quad (101)$$

Since the decomposition $(d(\mathbf{x}), \mathbf{a}(\mathbf{x}))$ is unique (see Lemma A1) and all the points $\mathbf{x} \in \Gamma_s$ share the same distance $d(\mathbf{x})$, then the mapping $\mathbf{a}_s := \mathbf{a}|_{\Gamma_s} : \Gamma_s \rightarrow \Gamma$ is invertible. Moreover, since $\mathbf{a}_0 = Id|_{\Gamma}$ (which implies $\|\nabla_{\Gamma} \mathbf{a}\| = 1$) and $\mathbf{a} \in \mathcal{C}^2(U)$ (see Remark A1), we can choose δ_0 small enough such that $0 < c \leq \|\nabla_{\Gamma_s} \mathbf{a}_s\| \leq C$. Hence, \mathbf{a}_s^{-1} is \mathcal{C}^2 as well, which implies that $\|\nabla_{\Gamma} \mathbf{a}_s^{-1}\| \leq C$. Hence by setting $\mathbf{y} = \mathbf{a}(\mathbf{x})$ we have

$$\int_{\Gamma_s} v^2(\mathbf{a}(\mathbf{x})) dx = \int_{\Gamma} v^2(\mathbf{y}) \|\nabla_{\Gamma} \mathbf{a}_s^{-1}(\mathbf{y})\| d\mathbf{y} \leq C\|v\|_{L^2(\Gamma)}^2, \quad (102)$$

where $\|\cdot\|$ is the Euclidean norm. By combining (101) and (102) we obtain the first inequality in (99), since δ_0 depends only on Γ . An application of the chain rule and Leibniz's rule yields

$$\nabla v_B(\mathbf{x}) = \nabla_{\Gamma} v(\mathbf{a}(\mathbf{x})) J\mathbf{a}(\mathbf{x}) \left(1 + \frac{d(\mathbf{x})}{\delta_0}\right) + v(\mathbf{a}(\mathbf{x})) \frac{\nabla d(\mathbf{x})}{\delta_0}.$$

Since $d(\mathbf{x})$ and $\mathbf{a}(\mathbf{x})$ are both \mathcal{C}^2 on the compact set $U_{\delta} \supset U_{\delta_0}$ and $-\delta_0 \leq d(\mathbf{x}) \leq 0$, we obtain

$$\|\nabla v_B(\mathbf{x})\| \leq C\|\nabla_{\Gamma} v(\mathbf{a}(\mathbf{x}))\| + \frac{C}{\delta_0} |v(\mathbf{a}(\mathbf{x}))|, \quad \forall \mathbf{x} \in U_{\delta_0}, \quad (103)$$

where $|\cdot|$ is the absolute value. Thanks to the continuous pasting in (100), it is easy to show that the bound (103) for the distributional gradient ∇v_B still holds on the junction Γ_{δ_0} between U_{δ_0} and $\Omega \setminus U_{\delta_0}$. From (A.9), (103) and the Young's inequality we have

$$\begin{aligned} \int_{\Omega} \|\nabla v_B(\mathbf{x})\|^2 d\mathbf{x} &\leq C \int_{-\delta_0}^0 ds \int_{\Gamma_s} \left(\|\nabla_{\Gamma} v(\mathbf{a}(\mathbf{x}))\|^2 + \frac{|v(\mathbf{a}(\mathbf{x}))|^2}{\delta_0^2} \right) d\mathbf{x} \\ &= \int_{-\delta_0}^0 ds \int_{\Gamma} \left(\|\nabla_{\Gamma} v(\mathbf{y})\|^2 + \frac{|v(\mathbf{y})|^2}{\delta_0^2} \right) \|\nabla_{\Gamma} \mathbf{a}_s^{-1}(\mathbf{y})\| d\mathbf{y} \\ &\leq C\delta_0 \int_{\Gamma} \left(\|\nabla_{\Gamma} v(\mathbf{y})\|^2 + \frac{|v(\mathbf{y})|^2}{\delta_0^2} \right) d\mathbf{y} \leq C \left(\|v\|_{L^2(\Gamma)}^2 + |v|_{H^1(\Gamma)}^2 \right), \end{aligned} \quad (104)$$

which proves the second inequality in (99). \square

Theorem 5 ($H^1(\Gamma)$, $L^2(\Gamma)$ and $L^2(\Omega)$ error bounds for the bulk Ritz projection). *Let Ω have a C^3 boundary. Then, for any $u \in H^{2+1/4}(\Omega)$ such that $\text{Tr}(u) \in H^2(\Gamma)$ and for h sufficiently small, it holds that*

$$\|u - (\mathcal{R}u)^\ell\|_{L^2(\Omega)} \leq Ch^2 \left(\|u\|_{H^2(\Omega)} + \|u\|_{H^{2+1/4}(\Omega)} \right), \quad (105)$$

$$\|u - (\mathcal{R}u)^\ell\|_{L^2(\Gamma)} + h|u - (\mathcal{R}u)^\ell|_{H^1(\Gamma)} \leq Ch^2 \|u\|_{H^2(\Gamma)}, \quad (106)$$

with C depending on Ω , γ_1 and γ_2 . In (105), the term in $H^{2+1/4}(\Omega)$ norm arises only in the simultaneous presence of curved boundaries and non-triangular boundary elements.

Proof. See Appendix B. □

In the following theorem we prove optimal convergence in $L^\infty([0, T], H^1(\Omega) \times H^1(\Gamma))$ norm for the spatially discrete parabolic problem (79), by harnessing the techniques used in [1], [24] and [28].

Theorem 6 (Convergence of the BSVEM for the parabolic case). *Assume that the kinetics q , r , s are C^2 and globally Lipschitz continuous (or at least Lipschitz on the range of the discrete solution). Assume that the exact solution (u, v) of the parabolic problem (2) is such that $u, u_t \in L^\infty([0, T]; H^{2+1/4}(\Omega))$ and $v, v_t, \text{Tr}(u), \text{Tr}(u_t) \in L^\infty([0, T]; H^2(\Gamma))$. Let (U, V) be the solution of (79). Then it holds that*

$$\|u - U^\ell\|_{L^\infty([0, T]; L^2(\Omega))} + \|v - V^\ell\|_{L^\infty([0, T]; L^2(\Gamma))} \leq Ch^2, \quad (107)$$

where the constant C depends on the diffusion coefficient d_u , the final time T and on the following norms:

- $\|(u, u_t)\|_{L^\infty([0, T]; H^2(\Omega))}, \|(v, v_t, \text{Tr}(u), \text{Tr}(u_t))\|_{L^\infty([0, T]; H^2(\Gamma))}$ in any case;
- $\|(u, u_t)\|_{L^\infty([0, T]; H^{2+1/4}(\Omega))}$ only in the simultaneous presence of curved boundaries and non-triangular boundary elements.

Proof. See Appendix B. □

5 Time discretisation of the parabolic problem

For the time discretisation of the semi-discrete formulation (83) of the parabolic problem (2) we use the IMEX (IMplicit-EXplicit) Euler method. The method approximates diffusion terms implicitly and reaction- and boundary terms explicitly, see for instance [28]. This choice is meant to make the implementation as simple as possible. However, if the boundary conditions and/or the reaction terms are linear, these can be approximated implicitly without involving any additional rootfinding step. We choose a timestep $\tau > 0$ and we consider the equally spaced discrete times $t_n := n\tau$, for $n = 0, \dots, N_T$, with $N_T := \lceil \frac{T}{\tau} \rceil$. For $n = 0, \dots, N_T$ we denote by ξ^n and η^n the numerical solution at time t_n . The IMEX Euler time discretisation of (83) reads

$$\begin{cases} M_\Omega \frac{\xi^{n+1} - \xi^n}{\tau} + K_\Omega \xi^{n+1} = M_\Omega q(\xi^n) + RM_\Gamma s(R^T \xi^n, \eta^n); \\ M_\Gamma \frac{\eta^{n+1} - \eta^n}{\tau} + K_\Gamma \eta^{n+1} = M_\Gamma (-s(R^T \xi^n, \eta^n) + r(R^T \xi^n, \eta^n)), \end{cases} \quad (108)$$

for $n = 0, \dots, N_T - 1$, where R is the reduction matrix introduced in (9). By solving for $\boldsymbol{\xi}^{n+1}$ and $\boldsymbol{\eta}^{n+1}$ we obtain the following time stepping scheme:

$$\begin{cases} (M_\Omega + \tau K_\Omega)\boldsymbol{\xi}^{n+1} = M_\Omega(\boldsymbol{\xi}^n + \tau q(\boldsymbol{\xi}^n)) + \tau R M_\Gamma s(R^T \boldsymbol{\xi}^n, \boldsymbol{\eta}^n); \\ (M_\Gamma + \tau K_\Gamma)\boldsymbol{\eta}^{n+1} = M_\Gamma(\boldsymbol{\eta}^n + \tau r(R^T \boldsymbol{\xi}^n, \boldsymbol{\eta}^n) - \tau s(R^T \boldsymbol{\xi}^n, \boldsymbol{\eta}^n)), \end{cases} \quad (109)$$

for $n = 0, \dots, N_T - 1$.

6 Benefits of polygonal meshes for BSPDEs

One of the benefits of using suitable polygonal elements is the reduction in computational complexity of the matrix assembly. This is useful especially for (i) time-independent problems and (ii) time-dependent problems on evolving domains, where matrix assembly might take the vast majority of the overall computational time.

As an example, given an arbitrarily shaped domain Ω with \mathcal{C}^1 boundary Γ , we construct a polygonal mesh designed for fast matrix assembly, by proceeding as follows. Suppose that the bulk Ω is contained in a square Q . We discretise Q with a Cartesian grid made up of square mesh elements and assume that at least one of such squares is fully contained in the interior of Ω (Fig. 4(a)). Then we discard the elements that are outside Q (Fig. 4(b)). Finally, we cut the elements that intersect the boundary Γ , thereby producing a discrete narrow band of irregular polygonal elements (highlighted in purple in Fig. 4(c)). The resulting mesh Ω_h has the important property that it is made up of equal square elements, except for the elements that are close to Γ , as we can see in Fig. 4(c). We now use this property to prove the reduction in computational complexity for matrix assembly. Let h be the meshsize of Ω_h . By construction, $h = h_Q$, where h_Q is the meshsize of the Cartesian grid. Of course, Ω_h is made up of $\mathcal{O}(h_Q^2) = \mathcal{O}(h^2)$ elements. However, by definition of Hausdorff dimension, the number of squares of Q that intersect Γ is $\mathcal{O}(h_Q) = \mathcal{O}(h)$, hence the number of non-square elements of Ω_h is only $\mathcal{O}(h)$. This implies that, when assembling the mass- and stiffness- matrices M_Ω and A_Ω , respectively, only $\mathcal{O}(h)$ element-wise local matrices must be actually computed, since the local matrices for a square element are pre-computed.

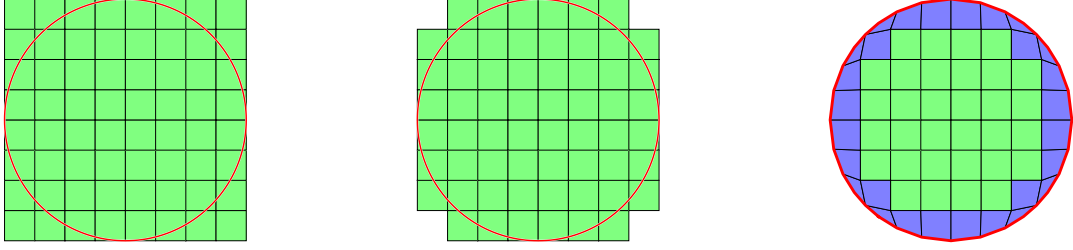
It is worth remarking that the advantage described in this section becomes even more striking in higher space dimension: if the embedding space has dimension $D \in \mathbb{N}$, then the procedure described in this section reduces the computational complexity of matrix assembly from $\mathcal{O}(h^D)$ to $\mathcal{O}(h^{D-1})$. Matrix assembly optimization can be also achieved through alternative approaches, such as cut FEM [16] or trace FEM [30]. However, in these works, the authors adopt a level set representation of the boundary Γ , which we do not need in this study, as we exploit the usage of arbitrary polygons to approximate Γ .

7 Numerical simulations

In this section we provide two numerical examples. In the first example, we show (i) that the BSVEM approximation of the elliptic problem (1) possesses optimal convergence in space and time and (ii) we illustrate the computational value and advantage of the optimised matrix assembly introduced in Section 6. In the second example, we show the application of the BSVEM-IMEX Euler fully discrete method to the parabolic bulk-surface wave pinning model studied in [21].

7.1 Experiment 1: The elliptic problem

We start by constructing an exact solution for the elliptic problem (1) on the unit circle $\Omega := \{(x, y) \in \mathbb{R}^2 | x^2 + y^2 = 1\}$ by using the fact that $-\Delta_\Gamma xy = 2xy$, i.e. the function $w(x, y) := xy$ is



(a) Step 1. The bulk Ω , enclosed by the red boundary Γ , is bounded by the green square Q , which is subdivided with a Cartesian grid. (b) Step 2. The mesh elements that are entirely outside Γ are discarded. (c) Step 3. The elements that intersect the surface Γ are cut, thereby producing the purple band of polygonal elements.

Figure 4: Generation of a polygonal bulk-surface mesh that allows for optimised matrix assembly.

an eigenfunction of the Laplace-Beltrami operator on the unit circumference $\Gamma = \partial\Omega$. Specifically, in (1) we choose the following load terms

$$f(x, y) := xy, \quad (x, y) \in \Omega, \quad \text{and} \quad g(x, y) := \left(2 + \frac{5(\alpha + 2)}{\beta}\right) xy, \quad (x, y) \in \Gamma,$$

where α and β are the parameters that appear in the model, such that the exact solution is given by

$$u(x, y) := xy, \quad (x, y) \in \Omega, \quad \text{and} \quad v(x, y) := \frac{\alpha + 2}{\beta} xy, \quad (x, y) \in \Gamma.$$

For illustrative purposes we choose $\alpha = 1$ and $\beta = 2$. We solve the problem on a sequence of five meshes similar to that of Figure 4 with decreasing meshsizes. For each mesh, we measure:

- the $L^2(\Omega)$ and $L^2(\Gamma)$ errors of the numerical solution and the respective experimental orders of convergence (EOC), that are quadratic in the meshsize;
- the total number of elements N_Ω and the total number of elements N_Γ that intersect the boundary, in order to show that the first is proportional to $\frac{1}{h^2}$, while the latter is proportional to $\frac{1}{h}$, as predicted in Section 6. This illustrates that only $O(\frac{1}{h})$ local matrices must be computed during matrix assembly, even if the mesh has $O(\frac{1}{h^2})$ elements.

In Fig. 5 we show the numerical solution on the finest mesh. In Table 1 we show the errors in L^2 norm, the EOC, the overall amount of elements per mesh and the number of elements that intersect the boundary Γ .

7.2 Experiment 2: The parabolic problem

In this section we compare the numerical solutions of the bulk-surface wave pinning (BSWP) model considered in [21, Fig. 4] obtained with BSFEM and BSVEM, respectively. In both cases, the time discretisation is carried out via IMEX Euler. The non-dimensionalised BSWP model seeks to find a

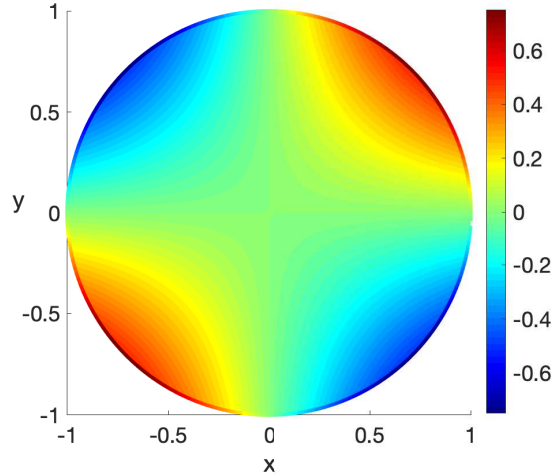


Figure 5: Experiment 1 for the elliptic problem (1). Numerical solution on the finest of the meshes listed in Table 1, with meshsize $h = 0.0442$.

Table 1: Experiment 1 for the elliptic problem (1), solved on a sequence of meshes of the type illustrated in Fig. 4. The experimental order of convergence in L^2 norm is two. Moreover, matrix assembly requires the computation of $N_\Gamma = O(\frac{1}{h})$ local matrices out of $N_\Omega = O(\frac{1}{h^2})$ elements.

h	$L^2(\Omega)$ error	EOC(Ω)	$L^2(\Gamma)$ error	EOC(Γ)	N_Ω	N_Γ
0.7071	2.0292e-02	-	4.7022e-02	-	16	12
0.3536	5.1901e-03	1.9671	1.2559e-02	1.9046	60	28
0.1768	1.4541e-03	1.8356	3.3709e-03	1.8975	224	60
0.0884	3.7226e-04	1.9658	8.7620e-04	1.9438	856	124
0.0442	9.6124e-05	1.9533	2.2551e-04	1.9581	3332	252

bulk concentration $b : \Omega \times [0, T] \rightarrow \mathbb{R}$ and a surface concentration $a : \Gamma \times [0, T] \rightarrow \mathbb{R}$ such that

$$\begin{cases} \varepsilon \frac{\partial b}{\partial t} b(\mathbf{x}, t) = \Delta b(\mathbf{x}, t), & \mathbf{x} \in \Omega, \\ \varepsilon \frac{\partial a}{\partial t} a(\mathbf{x}, t) = \varepsilon^2 \Delta_{\Gamma} a + f(a, b), & \mathbf{x} \in \Gamma, \\ -(\boldsymbol{\nu} \cdot \nabla b) = f(a, b), & \mathbf{x} \in \Gamma, \end{cases} \quad (110)$$

where the kinetic f is of the form

$$f(a, b) := \left(k_0 + \gamma \frac{a^2}{1 + a^2} \right) b - a. \quad (111)$$

We solve the BSWP model (110)-(111) on the unit circle

$$\Omega := \{(x, y) \in \mathbb{R}^2 | x^2 + y^2 \leq 1\}. \quad (112)$$

We choose the parameters of the model as follows:

$$\varepsilon^2 = 0.001, \quad k_0 = 0.05 \quad \text{and} \quad \gamma = 0.79. \quad (113)$$

The initial condition, plotted in the first row of Fig. 7, is as follows:

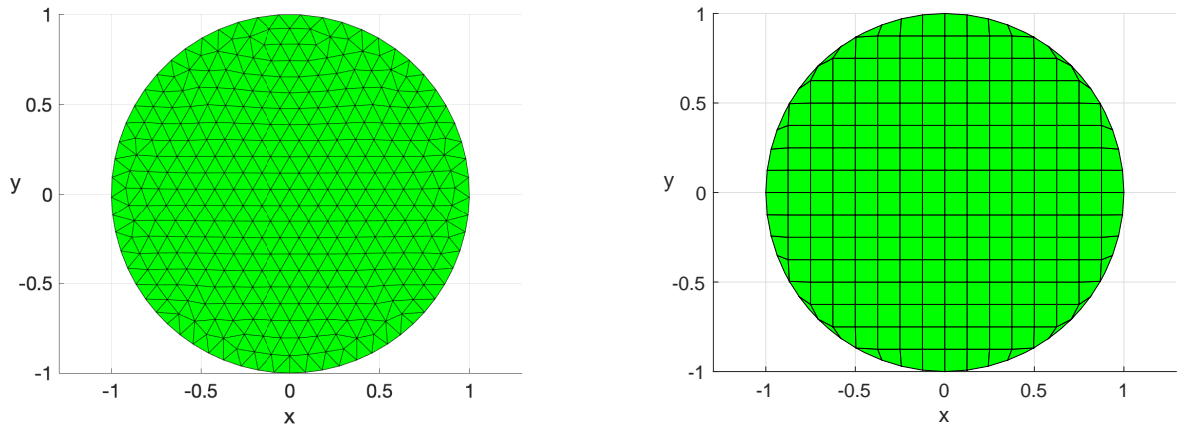
$$b(x, y, 0) = 2.487, \quad (x, y) \in \Omega, \quad (114)$$

$$a(x, y, 0) = 0.309 + 0.35(1 + \text{sign}(x)) \exp(-20y^2), \quad (x, y) \in \Gamma. \quad (115)$$

The final time is $T = 4.5$. For the BSFEM we take a triangular mesh, while for the BSVEM we take a polygonal mesh designed for optimised matrix assembly, as explained in Section 6. The details of these meshes are reported in Table 2. As we can see, on almost equal meshsizes, the BSVEM generates (i) significantly a large number of boundary nodes, which translates into better boundary approximation and (ii) less number of elements in the bulk, which implies faster matrix assembly. An illustrative coarser representation of the meshes typically used is shown in Fig. 6. For both spatial discretisations, the time discretisation is computed with timestep $\tau = 2e-3$.

Table 2: Details of the meshes used for the BSFEM and BSVEM, respectively. On almost equal meshsizes, the BSVEM mesh has significantly more boundary nodes (providing better boundary approximation) and less bulk elements (which simplifies matrix assembly) at the expense of a slightly higher overall number of bulk nodes compared to the BSFEM.

Spatial method	h (meshsize)	N (number of nodes)	M (number of boundary nodes)	$ \mathcal{E}_h $ (number of elements)
BSFEM	$3.10e-2$	5809	250	11366
BSVEM	$3.13e-2$	6754	364	6573



(a) Triangular mesh of the kind used for BSFEM.

(b) Discretisation mesh of the kind used for BSVEM.

Figure 6: Illustrative representation of the meshes used for the numerical experiments.

8 Conclusions

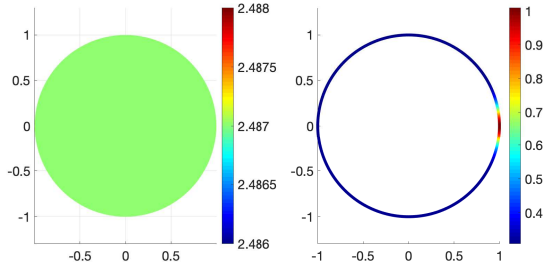
In this study, we have considered a bulk-surface virtual element method (BSVEM) for the numerical approximation of linear elliptic and semilinear parabolic coupled bulk-surface PDE problems on smooth bulk-surface domains. The proposed method simultaneously extends the BSFEM for bulk-surface RDSs [35] and the VEM for linear elliptic [5] and semilinear parabolic [1] bulk PDEs. Thanks to the usage of the interpolant operator and of a novel reduction matrix, the method possesses a simplified vector-matrix form that can be exploited also in the special case of the BSFEM considered in [35].

We have introduced polygonal bulk-surface meshes in two space dimensions and, under minimal mesh regularity assumptions, we have estimated the geometric error arising from domain approximation. Exactly as in the special case of the triangular bulk-surface meshes used in the BSFEM, the geometric error is $\mathcal{O}(h)$ in the bulk and $\mathcal{O}(h^2)$ on the surface, where h is the meshsize.

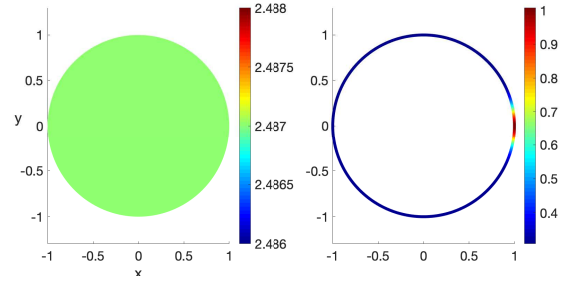
We have shown multiple advantages of polygonal bulk-surface meshes. First, suitable polygonal meshes reduce the asymptotic computational complexity of mesh generation and matrix assembly from $\mathcal{O}(h^2)$ to $\mathcal{O}(h)$, where h is the meshsize. Second, a portion of the surface can be approximated with a single polygonal element with many edges, which again translates into more efficient mesh generation and matrix assembly. Third -and not shown in this work- polygonal meshes allow for simple and efficient adaptive refinement strategies that would be impossible with triangular meshes. This aspect will be addressed in future studies.

We have introduced novel theory to address the challenges of the error analysis. First, we have shown that, if the exact solution is $H^{2+1/4}(\Omega)$ in the bulk and $H^2(\Gamma)$ on the surface, the lifting operator can be replaced with the Sobolev extension operator. Second, under suitable smoothness assumptions on the surface Γ , we have shown the existence of an L^2 -preserving inverse trace operator, i.e. an inverse trace operator that preserves the L^2 norm and the H^1 seminorm up to the same scale factor. Third, we have introduced a tailor-made Ritz projection in the bulk for the VEM that accounts for boundary conditions. By using the Sobolev extension and the L^2 -preserving inverse trace, we have shown that this Ritz projection fulfils optimal error bounds.

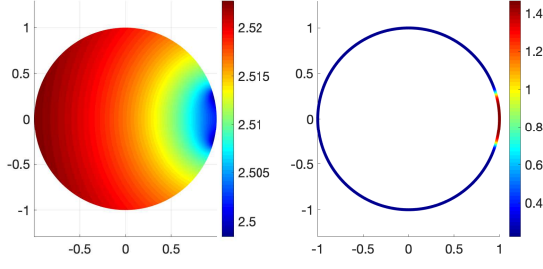
From the properties of our bulk-Ritz projection we have drawn two consequences. First, the lowest order bulk-VEM [5] retains optimal convergence even in the simultaneous presence of curved boundaries and non-zero boundary conditions, a result that lacked a rigorous justification in the



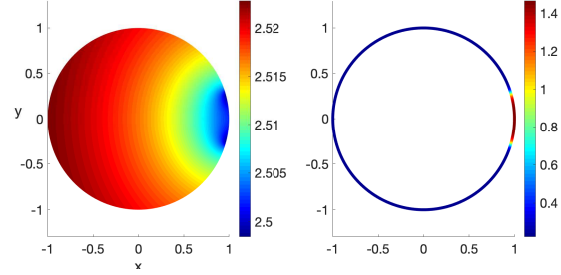
(a) BSFEM interpolant of the initial condition.



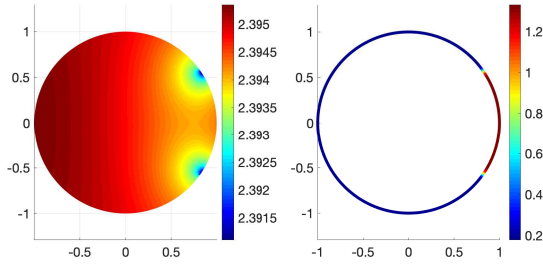
(b) BSVEM interpolant of the initial condition.



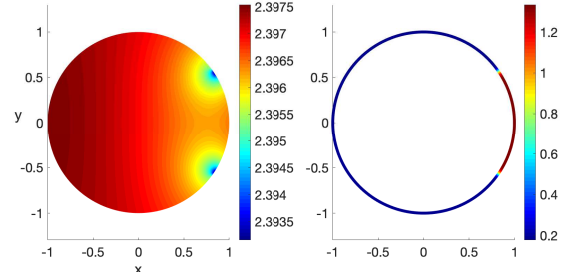
(c) BSFEM solution at time $t = 0.1$.



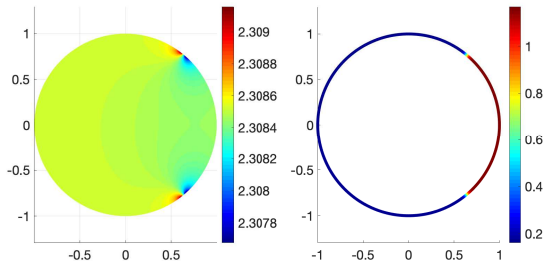
(d) BSVEM solution at time $t = 0.1$.



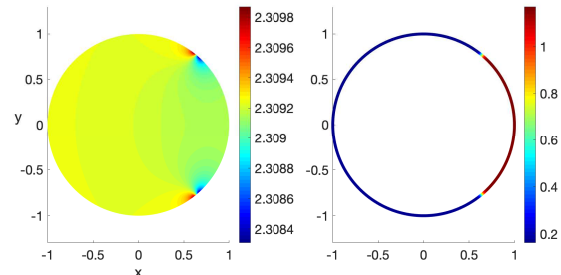
(e) BSFEM solution at time $t = 1$.



(f) BSVEM solution at time $t = 1$.



(g) BSFEM solution at time $t = 4.5$.



(h) BSVEM solution at time $t = 4.5$.

Figure 7: Comparisons between the BSFEM (left column) and the BSVEM (right column) solutions of the BSWP model (110)-(111). The solutions are qualitatively similar, but with a slightly shifted value range.

literature. Second, we have proven that the proposed BSVEM possesses an optimal error bound, that is $\mathcal{O}(h^2)$ in $L^\infty([0, T], L^2(\Omega) \times L^2(\Gamma))$ norm, where T is the final time.

We have provided two numerical examples to validate our findings in terms of (i) the convergence rate for the case of an elliptic problem and (ii) the computational advantages of polygonal meshes.

Acknowledgements

MF's research was partially funded by the Italian National Group of Scientific Computing (GNCS-INdAM) and by the University of Sussex. MF's and IS's research work has been performed under the auspices of the GNCS-INdAM. For the work AM is partly supported by funding from the European Union Horizon 2020 research and innovation programme under the Marie Skłodowska-Curie grant agreement No 642866, the Commission for Developing Countries, and was partially supported by a grant from the Simons Foundation. AM is a Royal Society Wolfson Research Merit Award Holder funded generously by the Wolfson Foundation. AM is a Distinguished Visiting Scholar to the Department of Mathematics, University of Johannesburg, South Africa.

References

- [1] D Adak, E Natarajan, and S Kumar. Convergence analysis of virtual element methods for semilinear parabolic problems on polygonal meshes. *Num Meth PDEs*, 35(1):222–245, 2019. doi:10.1002/num.22298.
- [2] R A Adams and J F Fournier. *Sobolev spaces*, volume 140. Elsevier, 2003. ISBN: 978-0-12-044143-3.
- [3] B Ahmad, A Alsaedi, F Brezzi, L D Marini, and A Russo. Equivalent projectors for virtual element methods. *CAMWA*, 66(3):376–391, 2013. doi:10.1016/j.camwa.2013.05.015.
- [4] P F Antonietti, L Beirão Da Veiga, S Scacchi, and M Verani. A C^1 virtual element method for the Cahn-Hilliard equation with polygonal meshes. *SIAM J Num Anal*, 54(1):34–56, 2016. doi:10.1137/15m1008117.
- [5] L Beirão Da Veiga, F Brezzi, A Cangiani, G Manzini, L D Marini, and A Russo. Basic principles of virtual element methods. *Math Mod Meth Appl Sci*, 23(01):199–214, 2013. doi:10.1051/m2an/2013138.
- [6] L Beirão Da Veiga, F Brezzi, and L D Marini. Virtual elements for linear elasticity problems. *SIAM J Num Anal*, 51(2):794–812, 2013. doi:10.1137/120874746.
- [7] L Beirão Da Veiga, F Dassi, and A Russo. High-order virtual element method on polyhedral meshes. *CAMWA*, 74(5):1110–1122, 2017. doi:10.1016/j.camwa.2017.03.021.
- [8] L Beirão Da Veiga, C Lovadina, and G Vacca. Divergence free virtual elements for the stokes problem on polygonal meshes. *ESAIM: M2AN*, 51(2):509–535, 2017. doi:10.1051/m2an/2016032.
- [9] L Beirão Da Veiga and G Manzini. A virtual element method with arbitrary regularity. *IMA J Num Anal*, 2013. doi:10.1093/imanum/drt018.
- [10] L Beirão Da Veiga, A Russo, and G Vacca. The virtual element method with curved edges. *ESAIM: M2AN*, 53(2):375–404, 2019. doi:10.1051/m2an/2018052.
- [11] M F Benedetto, S Berrone, and S Scialò. A globally conforming method for solving flow in discrete fracture networks using the virtual element method. *Fin Elem Anal Design*, 109:23–36, 2016. doi:10.1016/j.finel.2015.10.003.

- [12] N Benkemoun, A Ibrahimbegovic, and J-B Colliat. Anisotropic constitutive model of plasticity capable of accounting for details of meso-structure of two-phase composite material. *Computers & Structures*, 90:153–162, 2012. doi:10.1016/j.compstruc.2011.09.003.
- [13] S Bertoluzza, M Pennacchio, and D Prada. High order VEM on curved domains. *Rendiconti Lincei - Matematica e Applicazioni*, 30:391–412, 2019. doi:10.4171/RLM/853.
- [14] S Bianco, F Tewes, L Tajber, V Caron, O I Corrigan, and A M Healy. Bulk, surface properties and water uptake mechanisms of salt/acid amorphous composite systems. *Internat J Pharmaceutics*, 456(1):143–152, 2013. doi:10.1016/j.ijpharm.2013.07.076.
- [15] F Brezzi and L D Marini. Virtual element methods for plate bending problems. *Comp Meth Appl Mech Eng*, 253:455–462, 2013. doi:10.1016/j.cma.2012.09.012.
- [16] E Burman, P Hansbo, M Larson, and S Zahedi. Cut finite element methods for coupled bulk–surface problems. *Numerische Mathematik*, 133(2):203–231, 2016. doi:10.1007/s00211-015-0744-3.
- [17] A Cangiani, E H Georgoulis, and S Metcalfe. Adaptive discontinuous Galerkin methods for nonstationary convection–diffusion problems. *IMA J Num Anal*, 34(4):1578–1597, 2014. doi:10.1093/imanum/drt052.
- [18] J Chen. A memory efficient discontinuous Galerkin finite-element time-domain scheme for simulations of finite periodic structures. *Microwave and Optical Technology Letters*, 56(8):1929–1933, 2014. doi:10.1002/mop.28483.
- [19] A Y Chernyshenko, M A Olshanskii, and Y V Vassilevski. A hybrid finite volume–finite element method for bulk–surface coupled problems. *J Comput Phys*, 352:516–533, 2018. doi:10.1016/j.jcp.2017.09.064.
- [20] P G Ciarlet. *The Finite Element Method for Elliptic Problems*. Society for Industrial and Applied Mathematics, jan 2002. doi:10.1137/1.9780898719208.
- [21] D Cussteddu, L Edelstein-Keshet, J A Mackenzie, S Portet, and A Madzvamuse. A coupled bulk–surface model for cell polarisation. *J Theoret Biol*, Accepted for publication.
- [22] KY Dai, GR Liu, and TT Nguyen. An n-sided polygonal smoothed finite element method (nSFEM) for solid mechanics. *Fin Elem Anal Design*, 43(11):847–860, 2007. doi:10.1016/j.finel.2007.05.009.
- [23] E Di Nezza, G Palatucci, and E Valdinoci. Hitchhiker’s guide to the fractional Sobolev spaces. *Bulletin des Sciences Mathématiques*, 136(5):521–573, 2012. doi:10.1016/j.bulsci.2011.12.004.
- [24] G Dziuk and C M Elliott. Finite element methods for surface PDEs. *Acta Numerica*, 22:289–396, 2013. doi:10.1017/s0962492913000056.
- [25] C M Elliott and T Ranner. Finite element analysis for a coupled bulk–surface partial differential equation. *IMA J Num Anal*, 33(2):377–402, 2013. doi:10.1093/imanum/drs022.
- [26] C M Elliott and T Ranner. Evolving surface finite element method for the Cahn–Hilliard equation. *Numerische Mathematik*, 129(3):483–534, 2014. doi:10.1007/s00211-014-0644-y.

- [27] C M Elliott, T Ranner, and C Venkataraman. Coupled bulk-surface free boundary problems arising from a mathematical model of receptor-ligand dynamics. *SIAM J Math Anal*, 49(1):360–397, Jan 2017. doi:10.1137/15m1050811.
- [28] M Frittelli, A Madzvamuse, I Sgura, and C Venkataraman. Preserving invariance properties of reaction–diffusion systems on stationary surfaces. *IMA J Num Anal*, 39(1):235–270, 2017. doi:10.1093/imanum/drx058.
- [29] M Frittelli and I Sgura. Virtual element method for the Laplace-Beltrami equation on surfaces. *ESAIM: M2AN*, 52(3):965–993, 2018. doi:10.1051/m2an/2017040.
- [30] S Gross, M A Olshanskii, and A Reusken. A trace finite element method for a class of coupled bulk-interface transport problems. *ESAIM: M2AN*, 49(5):1303–1330, 2015. doi:10.1051/m2an/2015013.
- [31] B Kovács and C Lubich. Numerical analysis of parabolic problems with dynamic boundary conditions. *IMA J Num Anal*, 37(1):1–39, May 2017. doi:10.1093/imanum/drw015.
- [32] A A Lee, A Münch, and E Süli. Degenerate mobilities in phase field models are insufficient to capture surface diffusion. *Appl Phys Lett*, 107(8):081603, Aug 2015. doi:10.1063/1.4929696.
- [33] G MacDonald, J A Mackenzie, M Nolan, and R H Insall. A computational method for the coupled solution of reaction–diffusion equations on evolving domains and manifolds: Application to a model of cell migration and chemotaxis. *J Comp Phys*, 309:207–226, Mar 2016. doi:10.1016/j.jcp.2015.12.038.
- [34] J A Mackenzie, M Nolan, and R H Insall. Local modulation of chemoattractant concentrations by single cells: dissection using a bulk-surface computational model. *Interface Focus*, 6(5):20160036, 2016. doi:10.1098/rsfs.2016.0036.
- [35] A Madzvamuse and A H W Chung. The bulk-surface finite element method for reaction–diffusion systems on stationary volumes. *Finite Elem Anal Design*, 108:9–21, Jan 2016. doi:10.1016/j.finel.2015.09.002.
- [36] A Madzvamuse, A H W Chung, and C Venkataraman. Stability analysis and simulations of coupled bulk-surface reaction-diffusion systems. *Proc Royal Soc A: Math, Phys Eng Sci*, 471(2175):20140546–20140546, Feb 2015. doi:10.1098/rspa.2014.0546.
- [37] D Mora, G Rivera, and R Rodríguez. A virtual element method for the Steklov eigenvalue problem. *Math Mod Meth Appl Sci*, 25(08):1421–1445, 2015. doi:10.1142/s0218202515500372.
- [38] F Paquin-Lefebvre, W Nagata, and M J Ward. Pattern formation and oscillatory dynamics in a two-dimensional coupled bulk-surface reaction-diffusion system. *SIAM J Appl Dyn Sys*, 18(3):1334–1390, 2019. doi:10.1137/18m1213737.
- [39] A Rätz and M Röger. Symmetry breaking in a bulk–surface reaction–diffusion model for signalling networks. *Nonlinearity*, 27(8):1805–1827, Jul 2014. doi:10.1088/0951-7715/27/8/1805.
- [40] G Savaré. Regularity results for elliptic equations in Lipschitz domains. *J Funct Anal*, 152(1):176–201, 1998. doi:10.1006/jfan.1997.3158.

- [41] S.L. Sobolev. *Partial Differential Equations of Mathematical Physics*. Elsevier, 1964. doi:10.1016/c2013-0-01785-9.
- [42] E M Stein. *Singular Integrals and Differentiability Properties of Functions (PMS-30)*. Princeton University Press, 1971. doi:10.1515/9781400883882.
- [43] G Vacca. Virtual element methods for hyperbolic problems on polygonal meshes. *CAMWA*, 2016. doi:10.1016/j.camwa.2016.04.029.
- [44] G Vacca and L Beirão Da Veiga. Virtual element methods for parabolic problems on polygonal meshes. *Num Meth PDEs*, 31(6):2110–2134, 2015. doi:10.1002/num.21982.

Appendix A: Preliminary definitions and results

In this Appendix we provide preliminary definitions, results and notations adopted throughout the article. Unless explicitly stated, definitions and results are taken from [24].

A1. Surfaces and differential operators on surfaces

Let $\Omega \subset \mathbb{R}^2$ be a compact set such that its boundary $\Gamma := \partial\Omega \subset \mathbb{R}^2$ is a \mathcal{C}^k , $k \geq 2$ curve. Since Γ can be regarded as the zero level set of the *oriented distance function* $d : \mathbb{R}^2 \rightarrow \mathbb{R}$ defined by

$$d(\mathbf{x}) := \begin{cases} -\inf\{\|\mathbf{x} - \mathbf{y}\| : \mathbf{y} \in \Gamma\} & \text{if } \mathbf{x} \in \Omega; \\ 0 & \text{if } \mathbf{x} \in \Gamma; \\ \inf\{\|\mathbf{x} - \mathbf{y}\| : \mathbf{y} \in \Gamma\} & \text{if } \mathbf{x} \in \mathbb{R}^2 \setminus \Omega, \end{cases}$$

then the outward unit vector field $\boldsymbol{\nu} : \Gamma \rightarrow \mathbb{R}^3$ can be defined by

$$\boldsymbol{\nu}(\mathbf{x}) := \frac{\nabla d(\mathbf{x})}{\|\nabla d(\mathbf{x})\|}, \quad \mathbf{x} \in \Gamma, \tag{A.1}$$

see for instance [25].

Lemma A1 (Fermi coordinates). *If Γ is a \mathcal{C}^k , $k \geq 2$ surface, there exists an open neighbourhood $U \subset \mathbb{R}^3$ of Γ such that every $\mathbf{x} \in U$ admits a unique decomposition of the form*

$$\mathbf{x} = \mathbf{a}(\mathbf{x}) + d(\mathbf{x})\boldsymbol{\nu}(\mathbf{a}(\mathbf{x})), \quad \mathbf{a}(\mathbf{x}) \in \Gamma.$$

The maximal open set U with this property is called the Fermi stripe of Γ (see Fig. 1(a)), $\mathbf{a}(\mathbf{x})$ is called the normal projection onto Γ and $(\mathbf{a}(\mathbf{x}), d(\mathbf{x}))$ are called the Fermi coordinates of \mathbf{x} . The oriented distance function fulfils $d \in \mathcal{C}^k(U)$.

Proof. See [24]. □

Definition A1 ($\mathcal{C}^1(\Gamma)$ functions). *A function $u : \Gamma \rightarrow \mathbb{R}$ is said to be $\mathcal{C}^1(\Gamma)$ if there exist an open neighbourhood U of Γ and a \mathcal{C}^1 function $\hat{u} : U \rightarrow \mathbb{R}$ such that $\hat{u}|_{\Gamma} = u$, i.e. \hat{u} is a \mathcal{C}^1 extension of u off Γ .*

Definition A2 (Tangential gradient and tangential derivatives). *The tangential gradient $\nabla_\Gamma u$ of a function $u \in \mathcal{C}^1(\Gamma)$ is defined by*

$$\nabla_\Gamma u(\mathbf{x}) := \nabla \hat{u}(\mathbf{x}) - (\nabla \hat{u}(\mathbf{x}) \cdot \boldsymbol{\nu}(\mathbf{x}))\boldsymbol{\nu}(\mathbf{x}), \quad \mathbf{x} \in \Gamma. \quad (\text{A.2})$$

The result of the computation in (A.2) is independent of the choice of the extension \hat{u} . The components $D_x u$ and $D_y u$ of the tangential gradient $\nabla_\Gamma u$ are called the tangential derivatives of u .

Definition A3 ($\mathcal{C}^k(\Gamma)$ functions). *For $k \in \mathbb{N}$, $k > 1$, a function $u : \Gamma \rightarrow \mathbb{R}$ is said to be $\mathcal{C}^k(\Gamma)$ if it is $\mathcal{C}^1(\Gamma)$ and its tangential derivatives are $\mathcal{C}^{k-1}(\Gamma)$.*

Remark A1 (Regularity of normal projection). *Consider the function*

$$F(\mathbf{x}, \mathbf{y}) := \mathbf{y} - \mathbf{x} + d(\mathbf{x})\boldsymbol{\nu}(\mathbf{y}), \quad \mathbf{x} \in U, \mathbf{y} \in \Gamma.$$

Since $d \in \mathcal{C}^k(U)$ from Lemma A1 and $\boldsymbol{\nu} \in \mathcal{C}^{k-1}(\Gamma)$ from (A.1), then $F \in \mathcal{C}^{k-1}(\Omega \times \Gamma)$. Since the normal projection $\mathbf{a}(\mathbf{x})$ of $\mathbf{x} \in U$ can be regarded as the solution of the implicit equation $F(\mathbf{x}, \mathbf{a}(\mathbf{x})) = 0$, then $\mathbf{a} \in \mathcal{C}^{k-1}(U)$ as well.

Definition A4 (Laplace-Beltrami operator). *The Laplace-Beltrami operator $\Delta_\Gamma u$ of a function $u \in \mathcal{C}^2(\Gamma)$ is defined by*

$$\Delta_\Gamma u(\mathbf{x}) := D_x D_x u(\mathbf{x}) + D_y D_y u(\mathbf{x}), \quad \mathbf{x} \in \Gamma.$$

A2. Bulk- and surface function spaces

Definition A5 (Lebesgue function spaces). *Let $p \in [1, +\infty]$. For $u : \Omega \rightarrow \mathbb{R}$ and $v : \Gamma \rightarrow \mathbb{R}$ the bulk- and surface Lebesgue norms are defined by*

$$\|u\|_{L^p(\Omega)} := \begin{cases} \left(\int_\Omega |u|^p \right)^{1/p} & \text{if } p \in [1, +\infty); \\ \text{ess sup}_{\mathbf{x} \in \Omega} |u(\mathbf{x})| & \text{if } p = +\infty, \end{cases} \quad \|v\|_{L^p(\Gamma)} := \begin{cases} \left(\int_\Gamma |v|^p \right)^{1/p} & \text{if } p \in [1, +\infty); \\ \text{ess sup}_{\mathbf{x} \in \Gamma} |v(\mathbf{x})| & \text{if } p = +\infty, \end{cases}$$

respectively. The bulk- and surface Lebesgue function spaces are defined as

$$\begin{aligned} L^p(\Omega) &:= \{u : \Omega \rightarrow \mathbb{R} \mid \|u\|_{L^p(\Omega)} < +\infty\}; \\ L^p(\Gamma) &:= \{v : \Gamma \rightarrow \mathbb{R} \mid \|v\|_{L^p(\Gamma)} < +\infty\}, \end{aligned}$$

respectively.

Definition A6 (Sobolev function spaces). *Let $m \in \mathbb{N}$ and $p \in [1, +\infty]$. For $u : \Omega \rightarrow \mathbb{R}$ and $v : \Gamma \rightarrow \mathbb{R}$, the bulk- and surface Sobolev norms are defined by*

$$\|u\|_{W^{m,p}(\Omega)} := \begin{cases} \left(\sum_{|\alpha| \leq m} \|D_\alpha u\|_{L^p(\Omega)}^p \right)^{1/p} & \text{if } p \in [1, +\infty); \\ \max_{|\alpha| \leq m} \|D_\alpha u\|_{L^\infty(\Omega)} & \text{if } p = +\infty, \end{cases} \quad (\text{A.3})$$

$$\|v\|_{W^{m,p}(\Gamma)} := \begin{cases} \left(\sum_{|\alpha| \leq m} \|D_\alpha v\|_{L^p(\Gamma)}^p \right)^{1/p} & \text{if } p \in [1, +\infty); \\ \max_{|\alpha| \leq m} \|D_\alpha v\|_{L^\infty(\Gamma)} & \text{if } p = +\infty, \end{cases} \quad (\text{A.4})$$

respectively. The seminorms $|u|_{W^{m,p}(\Omega)}$ and $|v|_{W^{m,p}(\Gamma)}$ are defined by replacing $|\alpha| \leq m$ by $|\alpha| = m$ in (A.3)-(A.4). The bulk- and surface Sobolev function spaces are defined as

$$\begin{aligned} W^{m,p}(\Omega) &:= \{u : \Omega \rightarrow \mathbb{R} \mid \|u\|_{W^{m,p}(\Omega)} < +\infty\}; \\ W^{m,p}(\Gamma) &:= \{v : \Gamma \rightarrow \mathbb{R} \mid \|v\|_{W^{m,p}(\Gamma)} < +\infty\}, \end{aligned}$$

respectively. For $p = 2$ we will adopt the standard notations $H^m(\Omega) := W^{m,2}(\Omega)$ and $H^m(\Gamma) := W^{m,2}(\Gamma)$.

The following definition can be found in [23].

Definition A7 (Fractional Sobolev function spaces). *Let $s \in (0, 1)$ and $p \in [1, +\infty)$. For $u : \Omega \rightarrow \mathbb{R}$, the bulk- fractional Sobolev norm is defined by*

$$\|u\|_{W^{s,p}(\Omega)} := \left(\int_{\Omega} |u(\mathbf{x})|^p d\mathbf{x} + \int_{\Omega} \int_{\Omega} \frac{|u(\mathbf{x}) - u(\mathbf{y})|^p}{\|\mathbf{x} - \mathbf{y}\|^{2+sp}} d\mathbf{x} d\mathbf{y} \right)^{1/p}, \quad (\text{A.5})$$

with $\|\cdot\|$ being the Euclidean norm. If $s > 1$, $s \notin \mathbb{N}$, by decomposing s as $s = m + \sigma$, where $m \in \mathbb{N}$ and $\sigma \in (0, 1)$, the fractional Sobolev norm is defined as

$$\|u\|_{W^{s,p}(\Omega)} := \left(\|u\|_{W^{m,p}(\Omega)}^p + \sum_{|\alpha|=m} \|D_{\alpha} u\|_{W^{\sigma,p}(\Omega)}^p \right)^{1/p}. \quad (\text{A.6})$$

For any (integer or non-integer) $s \in [0, +\infty)$, the Sobolev-Slobodeckij space $W^{s,p}(\Omega)$ is defined as

$$W^{s,p}(\Omega) := \{u : \Omega \rightarrow \mathbb{R} \mid \|u\|_{W^{s,p}(\Omega)} < +\infty\}, \quad (\text{A.7})$$

where the norm $\|\cdot\|_{W^{s,p}(\Omega)}$ is understood as (A.3) or (A.6) according to whether s is an integer or a non-integer number.

Lemma A2 (Inclusion between fractional Sobolev spaces). *Let $\Omega \subset \mathbb{R}^2$ be a bounded domain with a C^1 boundary Γ , let $p \in [1, +\infty)$ and $s, s' \in [0, +\infty)$ such that $s < s'$. Then there exists a constant $C > 0$ depending on Ω and s such that*

$$\|u\|_{W^{s,p}(\Omega)} \leq C \|u\|_{W^{s',p}(\Omega)}, \quad (\text{A.8})$$

for all $u \in W^{s',p}(\Omega)$. Hence, $W^{s,p}(\Omega) \subset W^{s',p}(\Omega)$.

Proof. See [23]. □

A4. Fundamental results in bulk- and surface calculus

Theorem A1 (Co-area formula). *Let $\delta > 0$ such that the narrow band $U_{\delta} := \{\mathbf{x} \in \Omega \mid -\delta \leq d(\mathbf{x}) \leq 0\}$ is contained in the Fermi stripe U (see Fig. 1(a) for an illustration). For $-\delta \leq s \leq 0$ let Γ_s be the parallel surface defined by $\Gamma_s := \{\mathbf{x} \in \Omega \mid d(\mathbf{x}) = s\}$. For any $0 < \varepsilon \leq \delta$ it holds that*

$$\int_{U_{\varepsilon}} f(\mathbf{x}) d\mathbf{x} = \int_{-\varepsilon}^0 ds \int_{\Gamma_s} f(\sigma) d\sigma. \quad (\text{A.9})$$

Proof. See [24]. □

Theorem A2 (Narrow band trace inequality). *With the notations of the previous theorem, there exists $C > 0$ depending on Ω such that any $u \in H^1(\Omega)$ fulfils*

$$\|u\|_{L^2(U_\varepsilon)} \leq C\varepsilon^{\frac{1}{2}}\|u\|_{H^1(\Omega)}. \quad (\text{A.10})$$

Proof. See [25]. □

Theorem A3 (Trace theorem and inverse trace theorem). *Let $k \in \mathbb{N}$, $\frac{1}{2} < s \leq k$ and assume that the boundary Γ is a C^k curve.¹ Then there exists a bounded operator $\text{Tr} : H^s(\Omega) \rightarrow H^{s-\frac{1}{2}}(\Gamma)$, called the trace operator, such that $\text{Tr}(u) = u|_\Gamma$. The trace operator fulfils*

$$\|\text{Tr}(u)\|_{H^{s-\frac{1}{2}}(\Gamma)} \leq C\|u\|_{H^s(\Omega)}, \quad \forall u \in H^s(\Omega). \quad (\text{A.11})$$

The trace operator has a continuous inverse operator $\text{Tr}^{-1} : H^{s-\frac{1}{2}}(\Gamma) \rightarrow H^s(\Omega)$ called Babič inverse such that

$$\|\text{Tr}^{-1}(v)\|_{H^s(\Omega)} \leq C\|v\|_{H^{s-\frac{1}{2}}(\Gamma)}, \quad \forall v \in H^{s-\frac{1}{2}}(\Gamma). \quad (\text{A.12})$$

Proof. See [41] or [42]. □

A simple consequence of Theorem A3 is the following

Corollary A1 (Normal trace theorem). *Let $k \in \mathbb{N} \setminus \{1\}$, $\frac{3}{2} < s \leq k$ and assume that the boundary Γ is a C^k curve. There exists a bounded operator $Tn : H^s(\Omega) \rightarrow L^2(\Gamma)$, called the normal trace operator, such that $Tn(u) = \nabla u \cdot \mathbf{n}$, with \mathbf{n} being the outward unit normal vector field on Γ . The normal trace fulfils*

$$\|Tn(u)\|_{L^2(\Gamma)} \leq C\|u\|_{H^s(\Omega)}. \quad (\text{A.13})$$

Proof. Let $u \in H^s(\Omega)$, then $\nabla u \in H^{s-1}(\Omega)$. From Theorem A3 we have that $\text{Tr}(\nabla u) \in H^{s-3/2}(\Gamma)$. If $\|\cdot\|$ denotes the Euclidean norm in \mathbb{R}^2 , we have that

$$\begin{aligned} \|Tn(u)\|_{L^2(\Gamma)}^2 &= \int_\Gamma (\text{Tr}(\nabla u) \cdot \mathbf{n})^2 \leq \int_\Gamma \|\text{Tr}(\nabla u)\|^2 = \|\text{Tr}(\nabla u)\|_{L^2(\Gamma)}^2 \leq \|\text{Tr}(\nabla u)\|_{H^{s-3/2}(\Gamma)}^2 \\ &\leq C\|\nabla u\|_{H^{s-1}(\Omega)}^2 \leq C\|u\|_{H^s(\Omega)}^2. \end{aligned}$$

□

Theorem A4 (Sobolev extension theorem). *Assume that Ω has a Lipschitz boundary Γ , let $r \in \mathbb{N}$ and $p \in [1, +\infty]$. Then, for any function $u \in W^{r,p}(\Omega)$, there exists an extension $\tilde{u} \in W^{r,p}(\mathbb{R}^2)$ such that $\tilde{u}|_\Omega = u$ and*

$$\|\tilde{u}\|_{W^{r,p}(\mathbb{R}^2)} \leq C\|u\|_{W^{r,p}(\Omega)}, \quad (\text{A.14})$$

where C depends on Ω and r .

Proof. See [42]. □

Theorem A5 (Sobolev embeddings). *Assume that Ω has a Lipschitz boundary.*

- *If $0 < \gamma < 1$, then $H^{1+\gamma}(\Omega) \hookrightarrow C^{0,\gamma}(\Omega)$ is a continuous embedding, hence $\|u\|_{C^{0,\gamma}(\Omega)} \leq C_\gamma\|u\|_{H^{1+\gamma}(\Omega)}$. From the definition of the Hölder space $C^{0,\gamma}(\Omega)$ we have that*

$$\|u(\mathbf{x}) - u(\mathbf{y})\| \leq C_\gamma\|u\|_{H^{1+\gamma}(\Omega)}\|\mathbf{x} - \mathbf{y}\|^\gamma, \quad \text{a.e. } (\mathbf{x}, \mathbf{y}) \in \Omega^2. \quad (\text{A.15})$$

- *If $\varepsilon > 0$, then $H^{1+\varepsilon}(\Omega) \hookrightarrow C(\Omega)$ is a continuous embedding.*

Proof. See [2] for the case of integer-order Sobolev spaces and [23] for the fractional case. □

¹The original assumption is that Γ be a $C^{k-1,1}$ curve, meaning that its derivatives up to order $k-1$ are Lipschitz continuous. For simplicity, we make the stronger assumption that $\Gamma \in C^k$.

Appendix B: proofs of main theorems

Proof of Theorem 5

By assumption we have that $\text{Tr}(u) \in H^2(\Gamma)$. Since Γ is a \mathcal{C}^3 curve, then for all $F \in \mathcal{F}_h$, the normal projection $\mathbf{a} : F \rightarrow \mathbf{a}(F)$ is a \mathcal{C}^2 function, see Remark A1. Hence, $(u^{-\ell})|_F \in H^2(F)$ and

$$\sum_{F \in \mathcal{F}_h} \|u^{-\ell}\|_{H^2(F)} \leq C\|u\|_{H^2(\Gamma)}. \quad (\text{B.1})$$

From (27), (63), (96), and (B.1) we have that

$$\|u - (\mathcal{R}u)^\ell\|_{L^2(\Gamma)} = \|u - I_\Gamma(u^{-\ell})^\ell\|_{L^2(\Gamma)} \leq C\|u^{-\ell} - I_\Gamma(u^{-\ell})\|_{L^2(\Gamma_h)} \leq Ch^2\|u\|_{H^2(\Gamma)} \quad (\text{B.2})$$

$$|u - (\mathcal{R}u)^\ell|_{H^1(\Gamma)} = |u - I_\Gamma(u^{-\ell})^\ell|_{H^1(\Gamma)} \leq C|u^{-\ell} - I_\Gamma(u^{-\ell})|_{H^1(\Gamma_h)} \leq Ch\|u\|_{H^2(\Gamma)} \quad (\text{B.3})$$

From Lemma 7 there exists $e_B \in H^1(\Omega)$ such that $\text{Tr}(e_B) = \text{Tr}(u - (\mathcal{R}u)^\ell)$ and

$$\|e_B\|_{L^2(\Omega)} \leq \|\text{Tr}(u - (\mathcal{R}u)^\ell)\|_{L^2(\Gamma)} \leq Ch^2\|u\|_{H^2(\Gamma)}, \quad (\text{B.4})$$

$$|e_B|_{H^1(\Omega)} \leq \|\text{Tr}(u - (\mathcal{R}u)^\ell)\|_{H^1(\Gamma)} \leq Ch\|u\|_{H^2(\Gamma)}. \quad (\text{B.5})$$

We will use an adapted Aubin-Nitsche duality method. Consider the variational problem: find $\eta \in H_0^1(\Omega)$ such that

$$\int_\Omega \nabla \eta \cdot \nabla \varphi = \int_\Omega (u - (\mathcal{R}u)^\ell - e_B)\varphi, \quad \forall \varphi \in H_0^1(\Omega). \quad (\text{B.6})$$

Since $u - (\mathcal{R}u)^\ell - e_B \in H_0^1(\Omega)$, by elliptic regularity, the variational problem (B.6) has a unique solution $\eta \in H_0^3(\Omega)$ that fulfils

$$\|\eta\|_{H^2(\Omega)} \leq C\|(u - (\mathcal{R}u)^\ell - e_B)\|_{L^2(\Omega)}; \quad (\text{B.7})$$

$$\|\eta\|_{H^3(\Omega)} \leq C\|(u - (\mathcal{R}u)^\ell - e_B)\|_{H^1(\Omega)} \leq C|(u - (\mathcal{R}u)^\ell - e_B)|_{H^1(\Omega)}, \quad (\text{B.8})$$

thanks to Poincaré's inequality. By combining (97), (B.5) and (B.8) we have that

$$\|\eta\|_{H^3(\Omega)} \leq Ch\|u\|_{H^2(\Omega)} + Ch\|u\|_{H^{2+1/4}(\Omega)}. \quad (\text{B.9})$$

Since $u - (\mathcal{R}u)^\ell - e_B \in H_0^1(\Omega)$ we can choose $\varphi = u - (\mathcal{R}u)^\ell - e_B$ in (B.6) and we get

$$\begin{aligned} \|u - (\mathcal{R}u)^\ell - e_B\|_{L^2(\Omega)}^2 &= \int_\Omega \varphi^2 = \int_\Omega \nabla \eta \cdot \nabla \varphi = \int_\Omega \nabla \eta \cdot \nabla (u - (\mathcal{R}u)^\ell - e_B) \\ &= - \int_\Omega \nabla \eta \cdot \nabla e_B + \int_\Omega \nabla \eta \cdot \nabla (u - (\mathcal{R}u)^\ell) \end{aligned} \quad (\text{B.10})$$

We estimate the first term on the right-hand-side of (B.10) by using Green's identity, (A.13), (B.2), (B.4) and (B.7):

$$\begin{aligned} \left| \int_\Omega \nabla \eta \cdot \nabla e_B \right| &\leq \left| \int_\Omega e_b \Delta \eta \right| + \left| \int_\Gamma e_b \nabla \eta \cdot \mathbf{n} \right| \leq \|e_B\|_{L^2(\Omega)} \|\eta\|_{H^2(\Omega)} + \|e_B\|_{L^2(\Gamma)} \|Tn(\eta)\|_{L^2(\Gamma)} \\ &\leq \|e_B\|_{L^2(\Omega)} \|\eta\|_{H^2(\Omega)} + \|e_B\|_{L^2(\Gamma)} \|\eta\|_{H^2(\Omega)} \leq Ch^2\|(u - (\mathcal{R}u)^\ell - e_B)\|_{L^2(\Omega)}. \end{aligned} \quad (\text{B.11})$$

By using (29), (95) and the triangle inequality we estimate the the second term of the right-hand-side of (B.10) as follows

$$\begin{aligned}
& \int_{\Omega} \nabla \eta \cdot \nabla \left(u - (\mathcal{R}u)^\ell \right) \\
&= \int_{\Omega} \nabla \left(u - (\mathcal{R}u)^\ell \right) \cdot \nabla \left(\eta - I_{\Omega}(\tilde{\eta})^\ell \right) - \int_{\Omega} \nabla (\mathcal{R}u)^\ell \cdot \nabla I_{\Omega}(\tilde{\eta})^\ell + a_h(\mathcal{R}u, I_{\Omega}(\tilde{\eta})) \\
&\leq |u - (\mathcal{R}u)^\ell|_{H^1(\Omega)} |\eta - I_{\Omega}(\tilde{\eta})^\ell|_{H^1(\Omega)} - \int_{\Omega} \nabla (\mathcal{R}u)^\ell \cdot \nabla I_{\Omega}(\tilde{\eta})^\ell + a_h(\mathcal{R}u, I_{\Omega}(\tilde{\eta})) \\
&\leq |u - (\mathcal{R}u)^\ell|_{H^1(\Omega)} |\eta - I_{\Omega}(\tilde{\eta})^\ell|_{H^1(\Omega)} + Ch |(\mathcal{R}u)^\ell|_{H^1(\Omega_B^\ell)} |I_{\Omega}(\tilde{\eta})|_{H^1(\Omega_B^\ell)} \\
&\quad - \int_{\Omega_h} \nabla \mathcal{R}u \cdot \nabla I_{\Omega}(\tilde{\eta}) + a_h(\mathcal{R}u, I_{\Omega}(\tilde{\eta})) \\
&\leq C \left(|u - (\mathcal{R}u)^\ell|_{H^1(\Omega)} + h^{1/2} |u|_{H^1(\Omega_B^\ell)} \right) \left(|\eta - I_{\Omega}(\tilde{\eta})^\ell|_{H^1(\Omega)} + h^{1/2} |\eta|_{H^1(\Omega_B^\ell)} \right) \\
&\quad - \int_{\Omega_h} \nabla \mathcal{R}u \cdot \nabla I_{\Omega}(\tilde{\eta}) + a_h(\mathcal{R}u, I_{\Omega}(\tilde{\eta})),
\end{aligned} \tag{B.12}$$

where we have used $h < h_0$ in the last inequality. We are left to estimate the right-hand-side of (B.12) piecewise. First, from (A.10) and (97) we have that

$$|u - (\mathcal{R}u)^\ell|_{H^1(\Omega)} + h^{1/2} |u|_{H^1(\Omega_B^\ell)} \leq Ch \|u\|_{H^2(\Omega)} + Ch \|u\|_{H^{2+1/4}(\Omega)}, \tag{B.13}$$

Moreover, from (A.14), (A.10), (34), (56), (B.7) and (B.9) we have that

$$\begin{aligned}
& |\eta - I_{\Gamma}(\tilde{\eta})^\ell|_{H^1(\Omega)} + h^{1/2} |\eta|_{H^1(\Omega_B^\ell)} \leq C |\eta^{-\ell} - I_{\Gamma}(\tilde{\eta})|_{H^1(\Omega_h)} + Ch \|\eta\|_{H^2(\Omega)} \\
&\leq C |\eta^{-\ell} - \tilde{\eta}|_{H^1(\Omega_h)} + C |\tilde{\eta} - I_{\Gamma}(\tilde{\eta})|_{H^1(\Omega_h)} + Ch \|\eta\|_{H^2(\Omega)} \\
&\leq Ch^2 \|\eta\|_{H^3(\Omega)} + Ch \|\tilde{\eta}\|_{H^2(\Omega_h)} + Ch \|\eta\|_{H^2(\Omega)} \leq Ch \|\eta\|_{H^2(\Omega)} + Ch^2 \|\eta\|_{H^3(\Omega)} \\
&\leq Ch \|u - (\mathcal{R}u)^\ell - e_B\|_{L^2(\Omega)} + Ch^3 \|u\|_{H^2(\Omega)} + Ch^3 \|u\|_{H^{2+1/4}(\Omega)}.
\end{aligned} \tag{B.14}$$

Finally, we estimate the last two terms in (B.12) by adapting the approach used in [44, Lemma 3.1]: from (34), (41), (49), (56) and (B.7) we have

$$\begin{aligned}
& a_h(\mathcal{R}u, I_{\Gamma}(\tilde{\eta})) - \int_{\Omega_h} \nabla \mathcal{R}u \cdot \nabla I_{\Gamma}(\tilde{\eta}) \\
&= \sum_{E \in \mathcal{E}_h} \left(\int_E \nabla (\mathcal{R}u - \tilde{u}_\pi) \cdot \nabla (I_{\Gamma}(\tilde{\eta}) - \tilde{\eta}_\pi) - a_E(\mathcal{R}u - \tilde{u}_\pi, I_{\Gamma}(\tilde{\eta}) - \tilde{\eta}_\pi) \right) \\
&\leq \sum_{E \in \mathcal{E}_h} |\mathcal{R}u - \tilde{u}_\pi|_{H^1(E)} |I_{\Gamma}(\tilde{\eta}) - \tilde{\eta}_\pi|_{H^1(E)} \leq \left(Ch \|u\|_{H^2(\Omega)} + Ch \|u\|_{H^{2+1/4}(\Omega)} \right) Ch \|\eta\|_{H^2(\Omega)} \\
&= Ch^2 \left(\|u\|_{H^2(\Omega)} + \|u\|_{H^{2+1/4}(\Omega)} \right) \|u - (\mathcal{R}u)^\ell - e_B\|_{L^2(\Omega)},
\end{aligned} \tag{B.15}$$

By combining (B.10)-(B.15) and using (B.4) we get

$$\begin{aligned}
\|u - (\mathcal{R}u)^\ell\|_{L^2(\Omega)}^2 &\leq Ch^2 \left(\|u\|_{H^2(\Omega)} + \|u\|_{H^{2+1/4}(\Omega)} \right) \|u - (\mathcal{R}u)^\ell\|_{L^2(\Omega)} \\
&\quad + Ch^4 \left(\|u\|_{H^2(\Omega)} + \|u\|_{H^{2+1/4}(\Omega)} \right)^2,
\end{aligned} \tag{B.16}$$

with the terms in $H^{2+1/4}(\Omega)$ norm arising only in the simultaneous presence of curved boundaries and non-triangular boundary elements, which proves (105). \square

Proof of Theorem 6

We split the error as

$$(u, v) - (U^\ell, V^\ell) = ((u, v) - (\mathcal{R}u, \mathcal{R}v)^\ell) + ((\mathcal{R}u, \mathcal{R}v) - (U, V))^\ell =: (\rho_u, \rho_v) + (\theta_u, \theta_v). \quad (\text{B.17})$$

From (94), (97), (105) and (106), since the Ritz projections swap with time derivatives, we have that

$$\|(\text{Tr}(\rho_u), \text{Tr}(\rho_{u,t}), \rho_v, \rho_{v,t})\|_{L^2(\Gamma)} \leq Ch^2 \|(\text{Tr}(u), \text{Tr}(u_t), v, v_t)\|_{H^2(\Gamma)}; \quad (\text{B.18})$$

$$\|(\rho_u, \rho_{u,t})\|_{L^2(\Omega)} \leq Ch^2 \left(\| (u, u_t) \|_{H^2(\Omega)} + \| (u, u_t) \|_{H^{2+1/4}(\Omega)} \right). \quad (\text{B.19})$$

We are left to estimate the the norms of θ_u and θ_v . By using (2), (79), (95) and (B.17) we have the following error equation

$$\begin{aligned} & m_h \left(\frac{d}{dt} \theta_u^{-\ell}, \varphi \right) + d_u a_h \left(\theta_u^{-\ell}, \varphi \right) + \int_{\Gamma_h} \frac{d}{dt} \theta_v^{-\ell} \psi + d_v \int_{\Gamma_h} \nabla_{\Gamma_h} \theta_v^{-\ell} \cdot \nabla_{\Gamma_h} \psi \\ &= m_h \left(\frac{d}{dt} U, \varphi \right) - m_h \left(\frac{d}{dt} \mathcal{R}u, \varphi \right) + d_u a_h(U, \varphi) - d_u a_h(\mathcal{R}u, \varphi) \\ & \quad + \int_{\Gamma_h} \frac{d}{dt} V \psi - \int_{\Gamma_h} \frac{d}{dt} \mathcal{R}v \psi + d_v \int_{\Gamma_h} \nabla_{\Gamma_h} V \cdot \nabla_{\Gamma_h} \psi - d_v \int_{\Gamma_h} \nabla_{\Gamma_h} \mathcal{R}v \cdot \nabla_{\Gamma_h} \psi \\ &= m_h(I_\Omega q(\Pi^0 U), \varphi) - m_h \left(\frac{d}{dt} \mathcal{R}u, \varphi \right) - d_u a_h(\mathcal{R}u, \varphi) + \int_{\Gamma_h} I_\Gamma(s(U, V)) \varphi|_\Gamma \\ & \quad + \int_{\Gamma_h} I_\Gamma(r(U, V)) \psi - \int_{\Gamma_h} \frac{d}{dt} \mathcal{R}v \psi - d_v \int_{\Gamma_h} \nabla_{\Gamma_h} \mathcal{R}v \cdot \nabla_{\Gamma_h} \psi - \int_{\Gamma_h} I_\Gamma(s(U, V)) \psi \\ &= \underbrace{\int_{\Omega} \frac{d}{dt} u \varphi^\ell - m_h \left(\frac{d}{dt} \mathcal{R}u, \varphi \right)}_{T_1} + \underbrace{m_h(\Pi^0 I_\Omega q(\Pi^0 U), \varphi) - \int_{\Omega} q(u) \varphi^\ell}_{T_2} \\ & \quad + \underbrace{\int_{\Gamma} \frac{d}{dt} v \psi^\ell - \int_{\Gamma_h} \frac{d}{dt} \mathcal{R}v \psi}_{T_3} + \underbrace{\int_{\Gamma_h} I_\Gamma(r(U, V)) \psi - \int_{\Gamma} r(u, v) \psi^\ell}_{T_4} \\ & \quad + \underbrace{\int_{\Gamma_h} I_\Gamma(s(U, V)) (\text{Tr}(\varphi) - \psi) - \int_{\Gamma} (s(u, v)) (\text{Tr}(\varphi) - \psi)^\ell}_{T_5} \end{aligned} \quad (\text{B.20})$$

We now analyse terms $T_1 - T_5$ on the right hand side of (B.20) separately. For T_1 we use (A.10), (30) and (B.19):

$$\begin{aligned} T_1 &= \int_{\Omega} (u_t - (\mathcal{R}u_t)^\ell) \varphi^\ell + \int_{\Omega} (\mathcal{R}u_t)^\ell \varphi^\ell - \int_{\Omega_h} \mathcal{R}u_t \varphi + \int_{\Omega_h} \mathcal{R}u_t \varphi - m_h(\mathcal{R}u_t, \varphi) \\ &\leq \|u_t - (\mathcal{R}u_t)^\ell\|_{L^2(\Omega)} \|\varphi^\ell\|_{L^2(\Omega)} + Ch \|(\mathcal{R}u_t)^\ell\|_{L^2(\Omega_B^\ell)} \|\varphi^\ell\|_{L^2(\Omega_h^\ell)} + \int_{\Omega_h} \mathcal{R}u_t \varphi - m_h(\mathcal{R}u_t, \varphi) \\ &\leq \|u_t - (\mathcal{R}u_t)^\ell\|_{L^2(\Omega)} \|\varphi^\ell\|_{L^2(\Omega)} + Ch^2 \|(\mathcal{R}u_t)^\ell\|_{H^1(\Omega)} \|\varphi^\ell\|_{H^1(\Omega)} + \int_{\Omega_h} \mathcal{R}u_t \varphi - m_h(\mathcal{R}u_t, \varphi) \\ &\leq Ch^2 \left(\|u_t\|_{H^2(\Omega)} + \|u_t\|_{H^{2+1/4}(\Omega)} \right) \|\varphi^\ell\|_{H^1(\Omega)} + \int_{\Omega_h} \mathcal{R}u_t \varphi - m_h(\mathcal{R}u_t, \varphi). \end{aligned} \quad (\text{B.21})$$

We estimate the last term in (B.21) by using (A.14), (A.10), (25), (33), (41), (49) and (B.19):

$$\begin{aligned}
& \int_{\Omega_h} \mathcal{R}u_t \varphi - m_h(\mathcal{R}u_t, \varphi) \\
&= \sum_{E \in \mathcal{E}_h} \left(\int_E (\mathcal{R}u_t - \tilde{u}_{t,\pi}) \varphi - m_E(\mathcal{R}u_t - \tilde{u}_{t,\pi}, \varphi) \right) \leq \sum_{E \in \mathcal{E}_h} \|\mathcal{R}u_t - \tilde{u}_{t,\pi}\|_{L^2(E)} \|\varphi\|_{L^2(E)} \\
&\leq C \left(\|\rho_{u,t}\|_{L^2(\Omega)} + \|u_t^{-\ell} - \tilde{u}_t\|_{L^2(\Omega_h)} + \sum_{E \in \mathcal{E}_h} \|\tilde{u}_t - \tilde{u}_{t,\pi}\|_{L^2(E)} \right) \|\varphi^\ell\|_{L^2(\Omega)} \\
&\leq Ch^2 \left(\|u_t\|_{H^2(\Omega)} + \|u_t\|_{H^{2+1/4}(\Omega)} \right) \|\varphi^\ell\|_{L^2(\Omega)}.
\end{aligned} \tag{B.22}$$

By combining (B.23) and (B.22) we get

$$T_1 \leq Ch^2 \left(\|u_t\|_{H^2(\Omega)} + \|u_t\|_{H^{2+1/4}(\Omega)} \right) \|\varphi^\ell\|_{H^1(\Omega)}. \tag{B.23}$$

We estimate the second term by adapting the approach used in [1, Theorem 4.2]. From (A.10), (30), (33), (41), (46), (56)-(57) and (B.19), since q is \mathcal{C}^2 and Lipschitz continuous, we have that

$$\begin{aligned}
T_2 &= \int_{\Omega_h} \Pi^0 I_\Omega (q(\Pi^0 U) - q(\tilde{u})) \varphi + \int_{\Omega_h} \Pi^0 (I_\Omega q(\tilde{u}) - q(\tilde{u})) \varphi \\
&\quad + \int_{\Omega_h} (\Pi^0 q(\tilde{u}) - q(\tilde{u})) \varphi + \int_{\Omega_h} (q(\tilde{u}) - q(u^{-\ell})) \varphi + \int_{\Omega_h} q(u^{-\ell}) \varphi - \int_\Omega q(u) \varphi^\ell \\
&\leq C \|q(\Pi^0 U) - q(\tilde{u})\|_{L^2(\Omega_h)} \|\varphi\|_{L^2(\Omega_h)} + Ch^2 |q(\Pi^0 U) - q(\tilde{u})|_{2,\Omega,h} \|\varphi\|_{L^2(\Omega_h)} \\
&\quad + Ch^2 \|q(\tilde{u})\|_{H^2(\Omega_h)} \|\varphi\|_{L^2(\Omega_h)} + Ch^2 \|u\|_{H^2(\Omega)} \|\varphi\|_{L^2(\Omega_h)} + Ch \|q(u)\|_{L^2(\Omega_B^\ell)} \|\varphi^\ell\|_{L^2(\Omega_B^\ell)} \\
&\leq C \|U - \tilde{u}\|_{L^2(\Omega_h)} \|\varphi\|_{L^2(\Omega_h)} + Ch^2 (|U|_{H^1(\Omega)} + |\tilde{u}|_{H^1(\Omega_h)} + |\tilde{u}|_{H^2(\Omega_h)}) \|\varphi\|_{L^2(\Omega_h)} \\
&\quad + Ch^2 \left(\|u\|_{H^2(\Omega)} + \|u\|_{H^{2+1/4}(\Omega)} \right) \|\varphi^\ell\|_{L^2(\Omega)} + Ch^2 \|u\|_{H^1(\Omega)} \|\varphi^\ell\|_{H^1(\Omega)} \\
&\leq C \left(\|\theta_u\|_{L^2(\Omega)} + Ch^2 \|U\|_{H^1(\Omega_h)} + Ch^2 \|u\|_{H^2(\Omega)} + Ch^2 \|u\|_{H^{2+1/4}(\Omega)} \right) \|\varphi^\ell\|_{H^1(\Omega)}.
\end{aligned} \tag{B.24}$$

For the third term, from (A.10), (27), (32), and (B.18) we have that

$$\begin{aligned}
T_3 &= \int_\Gamma \frac{d}{dt} v \psi^\ell - \int_{\Gamma_h} \frac{d}{dt} v^{-\ell} \psi + \int_{\Gamma_h} \frac{d}{dt} v^{-\ell} \psi - \int_{\Gamma_h} \frac{d}{dt} \mathcal{R}v \psi \\
&\leq Ch^2 \|v_t\|_{L^2(\Gamma)} \|\psi^\ell\|_{L^2(\Gamma)} + C \|\rho_{v,t}\|_{L^2(\Gamma)} \|\psi^\ell\|_{L^2(\Gamma)} \leq Ch^2 \|v_t\|_{H^2(\Gamma)} \|\psi^\ell\|_{L^2(\Gamma)}
\end{aligned} \tag{B.25}$$

To estimate the fourth term we proceed as in (B.24). By using (32), (63)-(64), (B.1), (B.18), the \mathcal{C}^2 regularity and the Lipschitz continuity of r , we have that

$$\begin{aligned}
T_4 &= \int_{\Gamma_h} I_\Gamma \left(r(U, V) - r(u^{-\ell}, v^{-\ell}) \right) \psi + \int_{\Gamma_h} \left(I_\Gamma (r(u^{-\ell}, v^{-\ell})) - r(u^{-\ell}, v^{-\ell}) \right) \psi \\
&\quad + \int_{\Gamma_h} r(u^{-\ell}, v^{-\ell}) - \int_\Gamma r(u, v) \psi^\ell \leq C \|(U, V) - (I_\Gamma(u^{-\ell}), I_\Gamma(v^{-\ell}))\|_{L^2(\Gamma_h)} \|\psi\|_{L^2(\Gamma_h)} \\
&\quad + Ch^2 |r(u^{-\ell}, v^{-\ell})|_{2,\Gamma,h} \|\psi\|_{L^2(\Gamma_h)} + Ch^2 \|r(u, v)\|_{L^2(\Gamma)} \|\psi\|_{L^2(\Gamma)} \\
&\leq C (\|\theta_u, \theta_v\|_{L^2(\Gamma)} + \|(\rho_u, \rho_v)\|_{L^2(\Gamma)} + h^2 |(U, V)|_{H^1(\Gamma)} + h^2 \|(u, v)\|_{H^2(\Gamma)}) \|\psi^\ell\|_{L^2(\Gamma)} \\
&\leq C (\|\theta_u, \theta_v\|_{L^2(\Gamma)} \|\psi^\ell\|_{L^2(\Gamma)} + Ch^2 \|(u, v)\|_{H^2(\Gamma)} \|\psi^\ell\|_{L^2(\Gamma)}).
\end{aligned} \tag{B.26}$$

We estimate the fifth term as in (B.26) by also using (A.11):

$$\begin{aligned} T_5 &\leq C(\|(\theta_u, \theta_v)\|_{L^2(\Gamma)} + Ch^2\|(u, v)\|_{H^2(\Gamma)})\|\mathrm{Tr}(\varphi^\ell) - \psi^\ell\|_{L^2(\Gamma)} \\ &\leq C(\|(\theta_u, \theta_v)\|_{L^2(\Gamma)} + Ch^2\|(u, v)\|_{H^2(\Gamma)})(\|\varphi^\ell\|_{H^1(\Omega)} + \|\psi^\ell\|_{L^2(\Gamma)}). \end{aligned} \quad (\text{B.27})$$

By substituting (B.23)-(B.27) into the error equation (B.20), using Young's inequality and choosing $\varphi^\ell = \theta_u$, $\psi^\ell = \theta_v$ we have

$$\begin{aligned} &\frac{d}{dt}\|\theta_u\|_{L^2(\Omega)}^2 + d_u|\theta_u|_{H^1(\Omega)}^2 + \frac{d}{dt}\|\theta_v\|_{L^2(\Gamma)}^2 + d_v|\theta_v|_{H^1(\Gamma)}^2 \\ &\leq C(u, u_t, v, v_t, d_u)\left(h^4 + \|\theta_u\|_{L^2(\Omega)}^2 + \|\theta_v\|_{L^2(\Gamma)}^2\right) + d_u|\theta_u|_{H^1(\Omega)}^2, \end{aligned} \quad (\text{B.28})$$

which yields

$$\frac{d}{dt}\|\theta_u\|_{L^2(\Omega)}^2 + \frac{d}{dt}\|\theta_v\|_{L^2(\Gamma)}^2 \leq C(u, u_t, v, v_t, d_u)\left(h^4 + \|\theta_u\|_{L^2(\Omega)}^2 + \|\theta_v\|_{L^2(\Gamma)}^2\right). \quad (\text{B.29})$$

By applying Grönwall's lemma and accounting for the h^2 -accuracy of the initial conditions (80), we get the desired estimate. \square